UC Berkeley
UC Berkeley Previously Published Works

Title

Genome-scale and pathway engineering for the sustainable aviation fuel precursor isoprenol production in Pseudomonas putida

Permalink

https://escholarship.org/uc/item/3765n2n6

Authors

Banerjee, Deepanwita
Yunus, Ian S
Wang, Xi
et al.

Publication Date

2024-03-01

DOI

10.1016/j.ymben.2024.02.004

Copyright Information

Peer reviewed
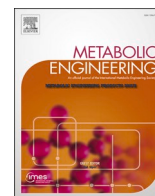
Genome-scale and pathway engineering for the sustainable aviation fuel precursor isoprenol production in *Pseudomonas putida*

Deepanwita Banerjee [a,b,1], Ian S. Yunus [a,b,1], Xi Wang [a,b,1], Jinho Kim [a,b], Aparajitha Srinivasan [a,b], Russel Menchavez [a,b], Yan Chen [a,b], Jennifer W. Gin [a,b], Christopher J. Petzold [a,b], Hector Garcia Martin [a,b], Jon K. Magnuson [a,c], Paul D. Adams [a,d], Blake A. Simmons [a,b], Aindrila Mukhopadhyay [a,b,e], Joonhoon Kim [a,c,**,1], Taek Soon Lee [a,b,*]

[a] *Joint BioEnergy Institute, 5885 Hollis St., Emeryville, CA, 94608, USA*
[b] *Biological Systems & Engineering Division, Lawrence Berkeley National Laboratory, Berkeley, CA, 94720, USA*
[c] *Energy Processes & Materials Division, Pacific Northwest National Laboratory, Richland, WA, 99354, USA*
[d] *Molecular Biophysics & Integrated Bioimaging Division, Lawrence Berkeley National Laboratory, Berkeley, CA, 94720, USA*
[e] *Environmental Genomics and Systems Biology Division, Lawrence Berkeley National Laboratory, Berkeley, CA, 94720, USA*

ARTICLE INFO

ABSTRACT

Sustainable aviation fuel (SAF) will significantly impact global warming in the aviation sector, and important SAF targets are emerging. Isoprenol is a precursor for a promising SAF compound DMCO (1,4-dimethylcy-clooctane) and has been produced in several engineered microorganisms. Recently, *Pseudomonas putida* has gained interest as a future host for isoprenol bioproduction as it can utilize carbon sources from inexpensive plant biomass. Here, we engineer metabolically versatile host *P. putida* for isoprenol production. We employ two computational modeling approaches (Bilevel optimization and Constrained Minimal Cut Sets) to predict gene knockout targets and optimize the "IPP-bypass" pathway in *P. putida* to maximize isoprenol production. Altogether, the highest isoprenol production titer from *P. putida* was achieved at 3.5 g/L under fed-batch conditions. This combination of computational modeling and strain engineering on *P. putida* for an advanced biofuels production has vital significance in enabling a bioproduction process that can use renewable carbon streams.

1. Introduction

Biological production of aviation fuels and their precursors from sustainable carbon sources stands to have a realistic impact on reducing CO_2 emissions, an increasingly critical aspect of addressing climate change (Baral et al., 2019a; Keasling et al., 2021). For this reason, several sustainable aviation fuel (SAF) targets and their precursors are being proposed, which include not only traditional ethanol-based fuels (Liew et al., 2022), but also novel high-energy multicyclic compounds possible via bioproduction, such as fuelimycin A (Cruz-Morales et al., 2022) and epi-isozizaene (Geiselman et al., 2020; Liu et al., 2018). One such important SAF precursor is isoprenol (a.k.a 3-methylbut-3-en-1-ol). Isoprenol is a commodity platform chemical and a vetted biogasoline (Department of Energy, U.S., 2021), and it is also the precursor to the jet

fuel 1,4-dimethyl cyclooctane (DMCO). Catalytic conversion of iso-prenol to DMCO has been shown at high efficiency (Baral et al., 2021) and establishing a carbon-efficient conversion of renewable carbon sources to isoprenol would enable a highly sustainable process (Baral et al., 2021) for DMCO.

While isoprenol production has been shown in model microbial hosts (*Escherichia coli* (Kang et al., 2019), *Corynebacterium glutamicum* (Sasaki et al., 2019), and *Saccharomyces cerevisiae* (Kim et al., 2021)), catabol-ically versatile microbes that consume a wider range of carbon com-pounds are essential to providing a cost-effective process (Baral et al., 2019a, 2019b). In the case of plant biomass conversion, there is an ur-gent need to demonstrate production of isoprenol in microbial systems that can catabolize both sugars and aromatics derived from lignocellu-losic biomass. *Pseudomonas putida* KT2440 is an ideal conversion host

* Corresponding author. Joint BioEnergy Institute, 5885 Hollis Street, Emeryville, CA, 94608. USA.
** Corresponding author. Joint BioEnergy Institute, 5885 Hollis St., Emeryville, CA, 94608, USA.
E-mail addresses: joonhoon.kim@pnnl.gov (J. Kim), tslee@lbl.gov (T.S. Lee).
[1] Equal Contributors.

with a versatile conversion profile and efficient genetic tools (Erickson et al., 2022; Martínez-García and de Lorenzo, 2019; Nikel and de Lorenzo, 2018; Weiland et al., 2022; Weimer et al., 2020). While prior works in model organisms (Kang et al., 2016; Tian et al., 2019) have achieved robust isoprenol titers, a microbial host such as *P. putida* KT2440 is a more likely candidate for the final deployment for isoprenol production as a SAF precursor. A less-commonly used laboratory host such as *P. putida*, however, is a far more challenging system to develop as a bioconversion platform. For instance, the most efficient route to isoprenol is through the heterologous mevalonate (MVA) pathway using an IPP-bypass that utilizes hydroxymethylglutaryl CoA (HMG-CoA) as the precursor (Kang et al., 2016). However, efforts in *P. putida* (Hernandez-Arranz et al., 2019) have shown that the mere MVA pathway overexpression did not provide any improvements over the native 2-C-methyl-D-erythritol 4-phosphate (MEP) pathway overexpression and both resulted in very low titers. A similar observation was also reported in cyanobacteria (Gao et al., 2016).

In a recent study, we were able to establish the MVA pathway in *P. putida* KT2440 (Wang et al., 2022) and define the necessary cultivation conditions to produce isoprenol in this host via the heterologous pathway. While this provides an excellent foundation for isoprenol production in *P. putida* KT2440, this microbes' unusual metabolic profile presents several challenges that need to be overcome. One issue is the catabolism of isoprenol itself, and its intermediates, by *P. putida* KT2440. Extensive functional genomics data have recently been accumulated for *P. putida* KT2440 and have revealed genes associated with degradation or catabolism of non-canonical carbon sources (e.g., levulinic acid (Rand et al., 2017), lysine (Thompson et al., 2019) and isoprenol (Thompson et al., 2020)), and also provided the hypotheses for host engineering targets to optimize the desired catabolism and minimize the undesired ones.

In addition to preventing the product degradation, the central carbon metabolism needs to be rewired to increase flux toward the heterologous isoprenol pathway whose precursor is acetyl-CoA. Since central metabolic intermediates such as acetyl-CoA and pyruvate are involved in many metabolic pathways, it is not trivial to select gene targets to pursue. Computationally driven metabolic engineering methods have gained interest during the last decade for predicting gene targets for overproduction of biochemicals (Maia et al., 2016). Such methods can predict strategies that may involve large numbers of genetic interventions (e.g. deletion, overexpression, or repression) to reach the predicted yields. Implementation of such strategies is sometimes challenging even with recent advances in synthetic biology and metabolic engineering techniques. To address this challenge and cover a larger solution space we used multiple computational strain design methods based on elementary mode analysis or bilevel optimization. The latest highly curated genome-scale metabolic model (GSMM) for *P. putida* (Nogales et al., 2020) enabled the use of these approaches and also highlighted the differences in metabolism from model microbes such as *E. coli*.

In this work, we employ two GSMM-guided approaches in combination with targeted edits and pathway improvements to enhance the production of the DMCO precursor, isoprenol, in *P. putida* KT2440 (Fig. 1). We first add the knowledge from functional genomics data sets (e.g., genes involved in isoprenol degradation) and the heterologous MVA pathway to update the GSMM (Fig. 2). We then use both Elementary mode analysis (EMA)-based methods (Terzer and Stelling, 2008; von Kamp and Klamt, 2017) and bilevel optimization (Opt)-based methods (Burgard et al., 2003; Ranganathan et al., 2010) to prioritize a subset of host genome targets that, when deleted, are predicted to enhance flux to isoprenol via the MVA route. We also use known edits such as deletion of the *pha* gene cluster (PP_5003 to PP_5005) (Czajka et al., 2022; Dong et al., 2019; Ouyang et al., 2007; Salvachúa et al., 2020; Wang et al., 2022) and other literature-based targets to further enhance isoprenol titers. Finally, we use proteomics to optimize the pathway configuration. Overall, our GSMM-guided approach allowed us to select and prioritize the intervention targets, and lead to over 3.5 g/L isoprenol from glucose in a minimal defined medium under fed-batch conditions. This titer is the highest reported for *P. putida* KT2440 and has vital significance in enabling a bioproduction process that can use renewable carbon streams as the starting material.
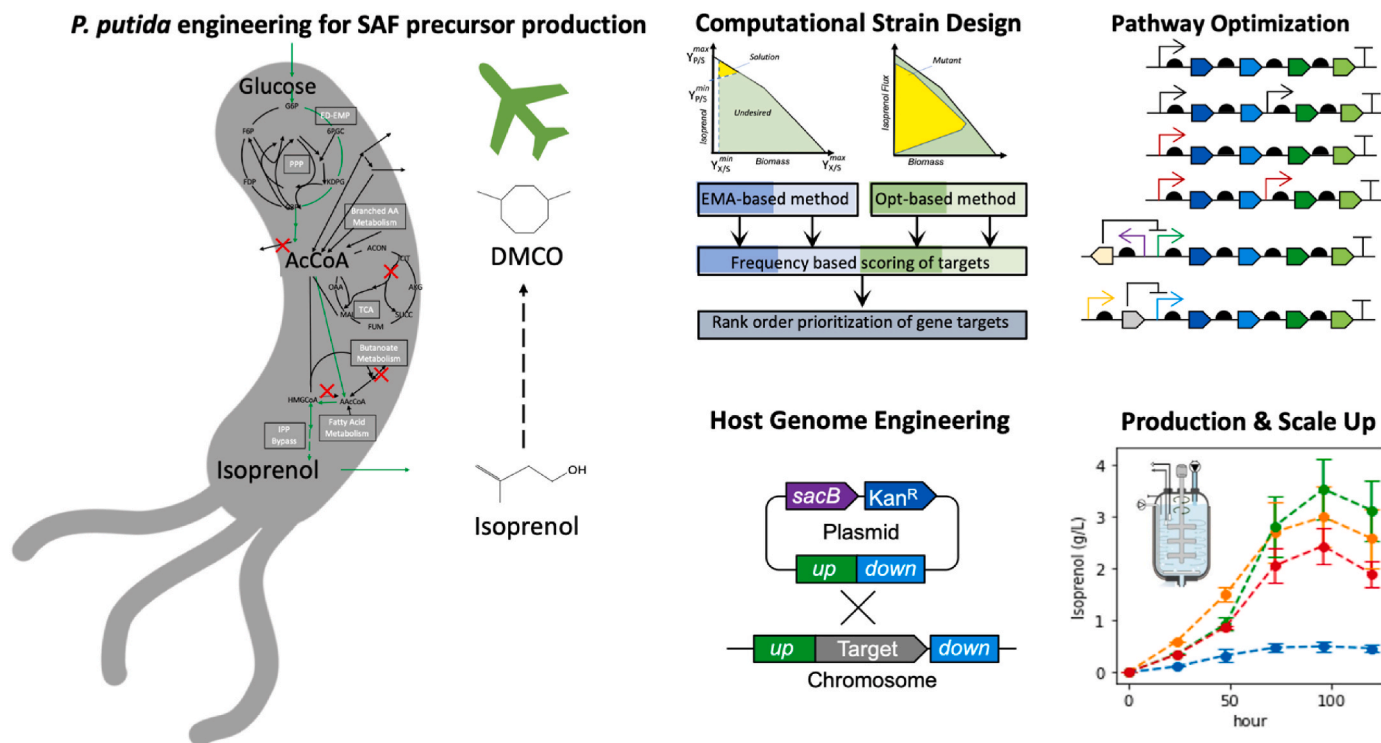

Fig. 1. Genome-scale metabolic and pathway engineering for production of the precursor of sustainable aviation fuel DMCO (1,4-dimethylcyclooctane), isoprenol, in *Pseudomonas putida*.
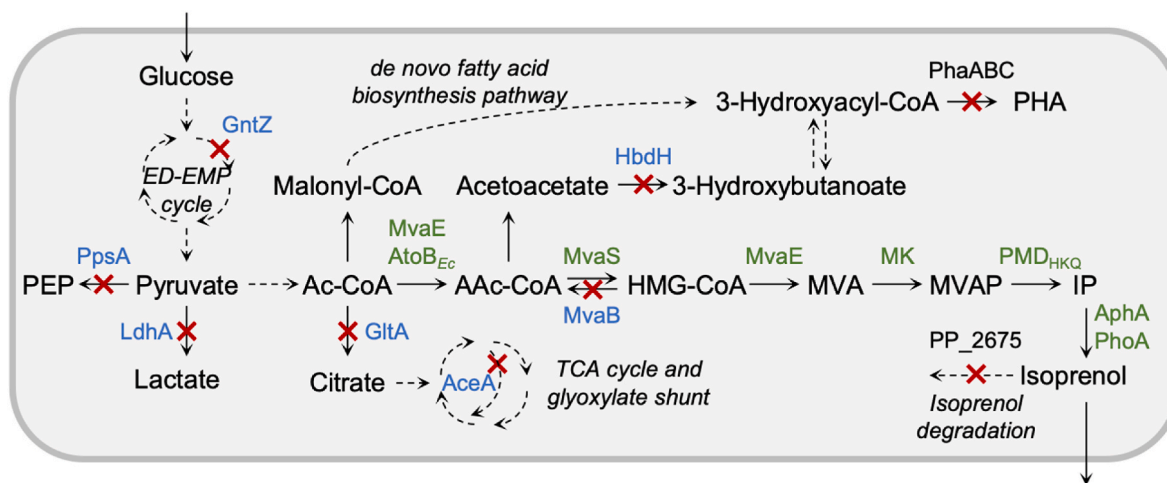
Fig. 2. Metabolic pathways for isoprenol production using IPP-bypass in *P. putida* KT2440. The gene knockout targets identified from genome-scale metabolic modeling are shown in blue. The heterologous genes for the IPP-bypass mevalonate pathway are shown in green.

2. Materials and methods

2.1. Computation of constrained minimal cut sets (cMCS) and elementary modes

Pseudomonas putida KT2440 genome scale metabolic model (GSMM) iJN1462 (Nogales et al., 2020) was used in this study although an upgraded GSMM for *P. putida* has been recently reported (Bujdoš et al., 2023). Aerobic conditions with glucose as the sole carbon source were used to model growth parameters. The ATP maintenance demand and glucose uptake were 0.97 mmol ATP/gDCW/h and 6.3 mmol glucose/gDCW/h, respectively. Constrained minimal cut sets (cMCS) were calculated using the MCS algorithm (von Kamp and Klamt, 2017) available as part of CellNetAnalyzer (version 2020.2) (Klamt et al., 2007). Excretion of byproducts was initially set to zero, except for the ones reported in literature as secreted metabolites specific to *P. putida* (gluconate and 2-ketogluconate (Nikel et al., 2015), 3-oxoadipate and catechol (Sudarsan et al., 2016), lactate and acetate (based on in house empirical evidence in some of our *P. putida* experiments as shown in Supplementary Fig. 1), and CO_2). We calculated the maximum theoretical yields (MTY) for isoprenol using glucose as the carbon source and the heterologous IPP bypass pathway (0.72 mol/mol of glucose). Additional inputs including minimum demanded product yield (10 %–85 % of MTY) and maximum demanded biomass yield at 10–25 % of maximum biomass yield were also specified in order to constrain the desired design space. The maximum size of MCS was kept at the default (i.e. 50 metabolic reactions). Knockouts of export reactions and spontaneous reactions were not allowed. With the specifications used herein, each calculated knockout strategy (cMCS) demands production of isoprenol even when cells do not grow. All cMCS calculations were done using API functions of CellNetAnalyzer (Klamt et al., 2007) on MATLAB 2017b platform using CPLEX 12.8 as the MILP solver. The different runs, respective number of cut sets and number of targeted reactions to satisfy coupling constraints are included in Supplementary File 1.

For elementary modes computation, a small model representing the central carbon metabolism of *Pseudomonas putida* KT2440 and the heterologous IPP bypass isoprenol production pathway was used to calculate elementary modes by *efmtool* (Terzer and Stelling, 2008).

2.2. Prediction of gene targets using Opt-based methods

The iJN1462 metabolic model was also used for OptKnock and OptForce. The model was first modified to fix mass or charge unbalanced reaction, remove duplicate reactions involving lipoamide dehydrogenase, remove the reactions catalyzed by genes on the TOL plasmid pWW0, remove the PPCK reaction by a pseudogene phosphoenolpyruvate carboxykinase PP_0253, and update the gene-protein-reaction association for the OAADC reaction from 2-dehydro-3-deoxy-phosphogluconate aldolase PP_1024 to oxaloacetate decarboxylase PP_1389. The modified model was augmented with the IPP-bypass pathway for isoprenol production (Supplementary File 2).

For OptKnock, the model was preprocessed to remove blocked reactions and metabolites and identify the reactions predicted to be essential for growth on glucose as a sole carbon source. The predicted essential reactions, spontaneous reactions, boundary reactions, and periplasmic transport reactions without associated genes were excluded from knockout targets. Several additional reactions were manually excluded from knockout targets to avoid undesired predictions (ATPM, CAT, CYO1_KT, CYTBO3_4pp, CYTCAA3pp, NADH16pp, NAt3_1p5pp, PItex, and PPK). The OptKnock problem was constructed using cobrapy (Ebrahim et al., 2013) and solved using CPLEX 12.8. Several iterations of OptKnock were run to identify a large number of knockout strategies using the solution pool and integer cuts. Another set of OptKnock solutions were obtained using a further constrained model where the secretion of other byproducts was blocked except for gluconate, 2-ketogluconate, and acetate assuming no significant byproduct formation (Supplementary File 3).

For OptForce, the model was also preprocessed to remove blocked reactions in glucose minimal media condition. The flux ranges for wild type were obtained by running flux variability analysis with constraints on glucose uptake, gluconate secretion, glucose dehydrogenase, gluconokinase, phosphogluconate dehydratase, pyruvate dehydrogenase, and citrate synthase taken from a previous study (Kukurugya et al., 2019). For isoprenol overproduction, we used 50 % of the theoretical maximum production as a pre-specified target to identify designs. All possible first and second-order necessary flux changes for overproduction were first identified and then used to identify the minimum set of interventions including flux increase, decrease, or knockouts. Several iterations of OptForce were run to identify a large number of designs by adding integer cuts using CPLEX 12.8 (Supplementary File 3).

2.3. Context specific models and flux variability analysis

For flux variability analysis, first context-specific models were generated using constraints derived from experimental data to create six different *P. putida* GSMMs to represent the 6 different *P. putida* strains engineered for isoprenol production in this study. Constraints for glucose uptake rate, isoprenol production rate as well as growth rate

were used. Next we performed flux variability analysis using *fluxvariabilityanalysis()* function in the COBRA Toolbox (Heirendt et al., 2019) on the MATLAB 2017b platform.

2.4. Strains and plasmid construction

All strains and plasmids used in this study are listed in Supplementary Table 1. Strains and plasmids along with their associated information have been deposited in the public domain of the JBEI Registry (https://public-registry.jbei.org) and are available from the authors upon request. Gene knockout of *P. putida* was performed based on the homologous recombination followed by a suicide gene (*sacB*) counterselection as previously described (Marx, 2008). The genotypes of gene-knockout mutants were confirmed by colony PCR using specific primers, followed by DNA sequencing (GENEWIZ, South San Francisco, CA, USA).

2.5. Isoprenol production in P. putida

P. putida KT2440 strains bearing isoprenol pathway plasmids (Supplementary Table 1) were used for isoprenol production. Starter cultures of all production strains were prepared by growing single colonies in LB medium containing 50 μg/mL kanamycin at 30 °C with 200 rpm shaking overnight. The starter cultures were diluted in 5 mL EZ rich defined medium (Teknova, CA, USA) containing 20 g/L D-glucose (2 %, w/v), 25 μg/mL kanamycin in 50-mL test tubes, and 0.5 mM IPTG or arabinose (2 %) was added to induce protein expression with OD_{600} at 0.4–0.6. The *P. putida* cultures were incubated in rotary shakers (200 rpm) at 30 °C for 48 h.

For isoprenol production runs on M9 minimal medium (Supplementary Table 2) with 2 % D-glucose, cryostocks were streaked to singles on LB agar plate with 50 μg/mL kanamycin at 30 °C. Single colonies were inoculated and grown overnight with shaking in 5 mL liquid LB medium supplemented with 50 μg/mL kanamycin at 30 °C and 200 rpm. Unless otherwise mentioned, all further cultivations were performed in the same format and conditions. 100 μL of these overnight LB grown cultures were back diluted into the minimal medium and grown for 24 h. A second back dilution enabled complete adaptation in the minimal medium. For the production runs, the cells were inoculated at an initial OD_{600} of 0.2 and the isoprenol production pathway was induced with 2 % arabinose immediately after inoculation. Samples were collected every 6 h until 72 h in triplicates and analyzed for growth (OD_{600}), isoprenol, residual glucose and organic acids.

The quantification of isoprenol was conducted as described in Kim et al. (2021) (Kim et al. (2021)). Briefly, 100 μL of ethyl acetate containing 1-butanol (30 mg/L) as the internal standard was added to 100 μL of liquid cultures. The mixture was vortexed at 3000 rpm for 15 min and subsequently centrifuged at $21,130 \times g$ for 3 min to separate the ethyl acetate phase from the aqueous phase. 1 μL of the ethyl acetate layer was analyzed by gas chromatography-flame ionization detection (GC-FID, Thermo Focus GC) equipped with a DB-WAX column (15 m, 0.32 mm inner diameter, 0.25 μm film thickness, Agilent, USA). The GC oven was programmed as follows: 40 °C – 100 °C at 15 °C/min, 100 °C – 230 °C at 40 °C/min finally, held at 230 °C for 2 min. The inlet temperature was 200 °C. Serial dilutions of isoprenol were prepared to quantify isoprenol in the samples.

The residual glucose and organic acids were analyzed using high performance liquid chromatography (HPLC, Agilent, USA) equipped with a refractive index detector (RID) and an Aminex HPX-87*X* column (Bio-Rad, USA) with 4 mM sulfuric acid as the mobile phase in the isocratic mode. The following conditions were used: Mobile phase flow rate: 0.6 mL/min, column at 60 °C, RID at 35 °C. Serial dilutions of glucose and organic acids were used to determine the concentration of glucose and organic acids in the samples. Data analysis was carried out on the ChemStation software (Agilent Technologies).

2.6. Targeted proteomics analysis of the isoprenol biosynthesis pathway proteins

Cell pellets of the engineered *P. putida* strains for isoprenol production were prepared for targeted proteomics analysis according to the previous report (Chen et al. (2019a)). Briefly, cells were resuspended in a solution with 80 μL of methanol and 20 μL of chloroform and thoroughly mixed by pipetting. Sixty microliters of water were subsequently added to the samples and mixed. Phase separation was induced with 5 min of centrifugation at $1000 \times g$. The methanol and water layers were removed, and then methanol (80 μL) was added to each well. The plate was centrifuged for 1 min at $100 \times g$, and then the supernatant layers were decanted. The protein pellets were resuspended in a 100 mM ammonium bicarbonate buffer supplemented with 20% methanol, and the protein concentration was determined by the DC assay (Bio–Rad). Proteins from each sample were reduced by addition of tris 2-(carboxyethyl) phosphine to 5 mM for 30 min at room temperature and followed by alkylation with iodoacetamide at 10 mM for 30 min at room temperature in the dark. Protein digestion with trypsin at 1 g/L concentration was accomplished with a 1:50 (w/w) trypsin/total protein ratio overnight. The multiple-reaction monitoring (MRM) assay was developed for relative quantification of isoprenol biosynthesis pathway proteins through a rapid method development workflow established previously (Chen et al., 2019b). Targeted proteomic analysis was performed on an Agilent 1290 UHPLC system coupled to an Agilent 6460 QqQ mass spectrometer according to an established protocol (dx.doi.org/10.17504/protocols.io.bf9xjr7n). Briefly, 20 g Peptides of each sample were separated on an Ascentis Express Peptide C18 column [2.7-mm particle size, 160 Å pore size, 5-cm length × 2.1-mm inside diameter (ID), coupled to a 5-mm × 2.1-mm ID guard column with the same particle and pore size, operating at 60 °C; Sigma-Aldrich] operating at a flow rate of 0.4 mL/min via the following gradient: initial conditions were 98% solvent A (0.1 % formic acid), 2 % solvent B (99.9 % acetonitrile, 0.1 % formic acid). Solvent B was increased to 5 % over 1 min, and was then increased to 40 % over 3.5 min. It was increased to 80 % over 0.5 min and held for 2.5 min at a flow rate of 0.6 mL/min, followed by a linear ramp back down to 2 % B at a flow rate of 0.4 mL/min over 0.5 min where it was held for 1 min to re-equilibrate the column to original conditions. The eluted peptides were ionized via an Agilent Jet Stream ESI source operating in positive ion mode. The MS raw data were acquired using Agilent MassHunter version B.08.02, and were analyzed by Skyline software version 21.20 (MacCoss Lab Software). The MRM method and data are available at Panoramaweb (Sharma et al., 2014) (https://panoramaweb.org/genome-scale-eng-SAF-p-putida.url) and at ProteomeXchange via identifier PXD039868.

2.7. Isoprenol production in fed-batch mode

For the isoprenol production in fed-batch mode, the strains were cultured in 5 mL LB medium with 50 μg/mL kanamycin at 30 °C. For the adaptation, the cell culture was diluted 50-fold in the fresh 5 mL modified M9 minimal medium two times. Then the seed culture was inoculated in the 1 L baffled flask including 100 mL modified M9 minimal medium at 30 °C and 200 rpm for 8 h. The cell culture was inoculated at OD_{600} 0.3 in the 2 L bioreactor (Biostat B, Sartorius, Germany) including the 1 L modified M9 minimal medium, which contained 6.8 g/L Na_2HPO_4, 3.0 g/L KH_2PO_4, 0.5 g/L NaCl, 20 mM NH_4Cl, 2 mM $MgSO_4$, 0.1 mM $CaCl_2$ and trace metal solution. The 1000 X trace metal solution (TEKNOVA, USA) consisted of 50 mM $FeCl_3$, 20 mM $CaCl_2$, 10 mM $MnCl_2$, 10 mM $ZnSO_4$, 2 mM $CoCl_2$, 2 mM $CuCl_2$, 2 mM $NiCl_2$, 2 mM Na_2MoO_4, 2 mM Na_2O_3Se, and 2 mM BH_3O_3. To produce isoprenol in the fed-batch fermentation, the dissolved oxygen (DO) and airflow were set to 20 % and 1 VVM (volume of air per volume of liquid per minute), respectively. The temperature was maintained at 25 °C and pH was maintained at 6.5 by supplementation with 25 % ammonia water. The isoprenol biosynthesis pathway was induced at OD_{600} 0.6–0.8 by 2 %

arabinose. The antifoam B was added to the bioreactor when required. To feed the additional carbon and nitrogen sources, a total of 80 g glucose and 15 g ammonium chloride in solution was continuously supplied using a Watson-Marlow DU520 peristaltic pump. The feeding flow rate was set to closely match the glucose consumption rate at the end of the batch phase. After the lag phase, the feeding flow rate was calculated following Korz's equation and increased every hour for a total of 6 h (Kang et al., 2019; Korz et al., 1995).

$$\mu(t) = \mu_{set} + \frac{1}{t - t_F} \, ln \, \frac{V(t)}{V_F}$$

For the exponential feeding, the glucose in the medium was measured consistently using the glucose meter (CVSHealth, USA) and high-performance liquid chromatography (HPLC), and feeding rate was set constant in order that the concentration of glucose was dropped below than 1 g/L in the medium. To extract the isoprenol from the off-gas, the exhaust line was connected directly to a bottle including the 1 L oleyl alcohol as extraction solvent. For quantification of isoprenol, 10 μL of oleyl alcohol layer was added to 990 μL of ethyl acetate containing 1-butanol (30 mg/L) as internal standard.

2.8. Isoprenol production using biomass hydrolysate

For the isoprenol production using biomass hydrolysate, the cholinium lysinate ionic liquid-pretreated sorghum hydrolysate was obtained from Joint BioEnergy Institute (JBEI) Deconstruction Division (Magurudeniya et al., 2021) and was used as a carbon source for the engineered *P. putida* strain. The sorghum hydrolysate was adjusted at pH 6.5 by sodium hydroxide and supplemented with 10X modified M9 salts at varying concentrations (0 %, 5 %, 10 %, 15 %, 20 %, 25 %, 30 %, and 35 % (v/v)). The glucose was added either as a sole carbon source or as co-substrate with sorghum hydrolysate and its concentration was adjusted to 20 g/L. Subsequently, we added 10 μL of 1 M MgSO₄, 5 μL of 100 mM CaCl₂, 2.5 μL of trace metal solution, and 50 μL of 1 M NH₄Cl to the modified M9 minimal medium. And the modified M9 minimal medium volume was adjusted to 5 mL. The strains were cultured in 5 mL LB medium with 50 μg/mL kanamycin at 30 °C overnight. To adapt the strain, the cell culture was diluted 50-fold in the fresh 5 mL modified M9 minimal medium two times. Then the seed culture was inoculated in the culture tubes including 5 mL modified M9 minimal medium supplemented sorghum hydrolysate at 30 °C and 200 rpm. The isoprenol biosynthesis pathway was induced at OD$_{600}$ 0.6–0.8 by 2 % arabinose. The isoprenol extraction was carried out using the same protocols as described above.

3. Results and discussion

3.1. Computational strain design for isoprenol production

For model-guided improvement of isoprenol production, we employed EMA-based approaches including Elementary Flux Modes (EFMs) (Terzer and Stelling, 2008) and Constrained Minimal Cut Sets (cMCS) (von Kamp and Klamt, 2017) as well as Opt-based approaches including OptKnock (Burgard et al., 2003; Segrè et al., 2002) and Opt-Force (Ranganathan et al., 2010) using the GSMM for *P. putida* iJN1462 (Nogales et al., 2020) augmented with the heterologous MVA pathway (Supplementary File 2) and a central metabolic model for *P. putida* with a lumped reaction for the heterologous MVA pathway (Supplementary File 4). Preliminary computational strain design results showed that growth-coupled production of isoprenol requires the deletion of 9 or more metabolic reactions in *P. putida* (Supplementary File 3). However, it is not clear from computational predictions which genes are more important for increasing isoprenol production and therefore should be knocked out with high priority since the growth-coupled production does not happen *in silico* with the deletion of a subset of identified reactions. To this end, we generated a large number of

computational designs using EMA-based and Opt-based methods and calculated the frequency of knockout targets appearing in the designs by each method. The frequency was used to calculate the rank order of targets for each method, and the rank order from different methods was combined to calculate the final score. Our assumption was that certain targets can be more important for improving isoprenol production (e.g., due to higher fluxes or key branch points) than others and thus will appear more frequently in a diverse set of computational designs. By generating a large number of designs using multiple computational methods and combining them using a rank-based ensemble approach, we aimed to identify such crucial targets and prioritize them for the experimental construction of knockout strains. Although the computational model requires the deletion of all targets from a design to see improved isoprenol production, we hypothesized that the deletion of a subset consisting of these crucial targets will still lead to improved isoprenol production.

For the EMA-based methods, we first calculated EFMs using the central metabolic model. Each EFM is a minimal set of reactions carrying flux under the defined glucose minimal medium condition for growth as well as isoprenol production. A total of 360,475 EFMs were computed of which only 276 EFMs were selected that carried a flux through the biomass, ATP maintenance, glucose uptake, and isoprenol production reactions. A frequency-based scoring was used to prioritize targets, from 276 different computed EFMs (Supplementary File 1). Further we used cMCS to compute growth-coupled strategies for isoprenol production using the GSMM. From a total of 60 cMCS runs, we enumerated 4950 feasible cMCS cut set designs. We used frequency-based scoring to prioritize targets from the feasible cMCS designs that were computed for isoprenol and its precursors HMG-CoA, DMAPP or IPP (Supplementary File 1).

For the Opt-based methods, OptKnock was first used to find knockouts to couple isoprenol production to growth using the GSMM. A total of 157 OptKnock solutions were initially collected and pre-processed to 120 solutions by removing redundant solutions. In addition, we constrained the model by blocking the secretion of byproducts except for experimentally observed ones (e.g., gluconate, 2-ketogluconate, and acetate) to find another set of designs. Using the constrained model, 377 OptKnock solutions were obtained and pre-processed to 263 solutions. OptForce was next used to identify strategies to improve isoprenol production using the GSMM. A total of 50 OptForce solutions were obtained, but we found that they consisted mostly of routes that increase or decrease flux and included only 9 knockout targets with low frequencies. Therefore, we decided to use the OptKnock solutions from two simulations to calculate the frequency for scoring gene targets (Supplementary File 3).

Finally, we combined scores from EMA-based and Opt-based predictions to arrive at the top 8 priority gene targets for experimental implementation (Table 1 and Fig. 2). The first two priority gene targets (*mvaB* and *hbdH*) were involved in the degradation of endogenous metabolites (HMG-CoA and acetoacetyl-CoA) that also participate in the heterologous MVA pathway. The other priority gene targets were involved in central carbon metabolism including the pentose phosphate pathway (*gntZ*), pyruvate metabolism (*ldhA* and *ppsA*), and TCA cycle (*gltA* and *aceA*). Although some of the predicted gene targets were involved in the degradation of intermediates, our computational approach guides the metabolic engineering process by prioritizing gene targets predicted from well-established algorithms. Such an approach is needed to facilitate strain construction when a computational design contains many gene targets.

3.2. Experimental implementation of metabolic rewiring for isoprenol production

To experimentally verify the model-predicted targets, *P. putida* Δ*phaABC* strain (XW01, see Supplementary Table 2 for the list of strains) was used as a background strain to perform gene knockouts. This strain

Table 1

Priority Targets based on EMA-based and Opt-based approaches for experimental validation.

Reaction ID	Reaction Name	Gene Association	Note[a]
HMGL	Hydroxymethylglutaryl-CoA lyase	*mvaB* (PP_3540)	1st target by combined score
BDH	3-hydroxybutyrate dehydrogenase	*hbdH* (PP_3073)	2nd target by combined score
GND	Phosphogluconate dehydrogenase	*gntZ* (PP_4043)	3rd target by combined score
LDH_D	D-lactate dehydrogenase	*ldhA* (PP_1649)	High cMCS/EFM score, low OptKnock score
PPS	Phosphoenolpyruvate synthase	*ppsA* (PP_2082)	High cMCS/EFM score, low OptKnock score
CS	Citrate synthase	*gltA* (PP_4194)	High OptKnock score, low cMCS/EFM score
ICL	Isocitrate lyase	*aceA* (PP_4116)	High OptKnock score, low cMCS/EFM score

[a] See **Supplementary File 5** for details.

has shown the highest isoprenol level in *P. putida* (104 mg/L, XW11 strain) when using the IPP-bypass MVA pathway via a plasmid (pXW1, see Supplementary Table 1 for the list of plasmids) in our previous work (Wang et al., 2022). According to the model-predicted targets (Table 1), we constructed single and multiple gene knockout strains (Fig. 3a). We started with the PP_3540/*mvaB* gene as it encodes for HMG-CoA lyase which catalyzes a reaction transforming HMG-CoA into acetoacetate and acetyl-CoA, hence competing for HMG-CoA, a key precursor in mevalonate synthesis. The knockout of *mvaB* improved isoprenol production up to 164 mg/L, which increased 1.6-fold compared with the starter strain XW11 (Fig. 3b).

Using this double-knockout strain (ΔphaABC ΔmvaB) as a base, we performed a second round of gene knockouts with PP_4116/*aceA*

(isocitrate lyase), PP_4043/*gntZ* (6-phosphogluconate dehydrogenase), and PP_3073/*hbdH* (3-hydroxybutyrate dehydrogenase) (Fig. 3a). While the knockout of *aceA* (XW13) or *gntZ* (XW14) significantly decreased isoprenol production to 14–15 mg/L, the *hbdH* knockout (XW15) improved isoprenol production up to 241 mg/L, a 2.3-fold increase from the XW11 strain and 1.5-fold increase from the XW12 strain, respectively (Fig. 3b). As 3-hydroxybutyrate dehydrogenase (*hbdH*) catalyzes the conversion between 3-hydroxybutyrate and acetoacetate, the success of *hbdH* knockout in increasing isoprenol production may be attributed to the removal of a competing pathway of acetoacetyl-CoA, the first metabolite in the MVA pathway. Isocitrate lyase (*aceA*) converts isocitrate to glyoxylate, and 6-phosphogluconate dehydrogenase (*gntZ*) is a key enzyme at the shunt of the pentose phosphate pathway and the ED pathway. They are both involved in central carbon metabolism and the failure of these two knockouts in isoprenol improvement indicates that central carbon metabolism may require a significant rewiring by combinations of gene knockouts rather than a single gene deletion. Thus, engineering multiple gene knockouts in one strain may still be required to further improve isoprenol production.

Therefore, for the third round of knockouts, we picked the highest producer with the triple knockouts (ΔphaABC ΔmvaB ΔhbdH, XW15) as a base, and performed the knockout of the genes involved in central carbon metabolism, *gltA* (citrate synthase), *aceA* (isocitrate lyase), and *gntZ* (6-phosphogluconate dehydrogenase) (Fig. 3a). Since citrate synthase is the first enzyme connecting glycolysis and the TCA cycle, it plays an important role in central carbon and energy metabolism. In *P. putida* KT2440, citrate synthase derives 3-fold more carbon flux from acetyl-CoA to TCA cycle compared with *E. coli* (Wang et al., 2022). Thus, the knockout of *gltA* may limit the flux out of acetyl-CoA, which is desirable to support the MVA pathway flux and isoprenol production. However, experimental results (Fig. 3b) showed that the deletion of *gltA* (XW16) significantly compromised cell growth and eventually lowered isoprenol production (19 mg/L). Given that the clear detriment of cell growth, *gltA* was not continued with a further round of gene knockout. Adaptive

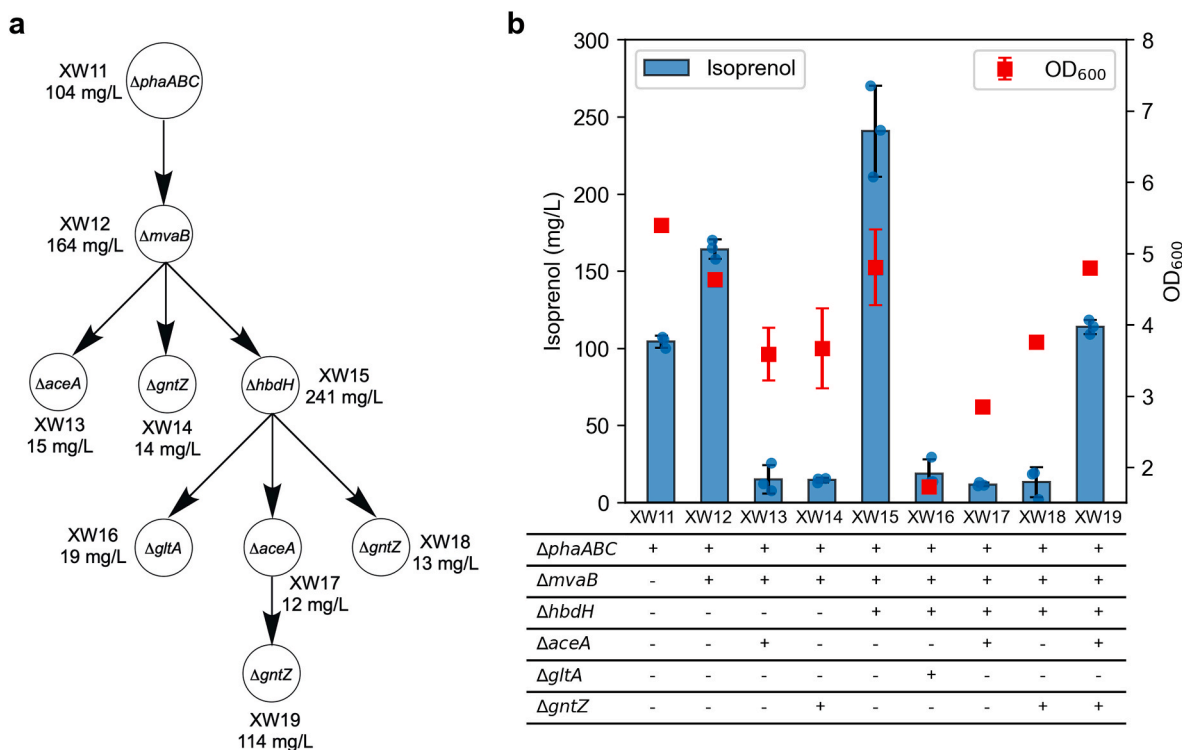|	XW11	XW12	XW13	XW14	XW15	XW16	XW17	XW18	XW19
ΔphaABC	+	+	+	+	+	+	+	+	+
ΔmvaB	-	+	+	+	+	+	+	+	+
ΔhbdH	-	-	-	-	+	+	+	+	+
ΔaceA	-	-	+	-	-	+	-	+
ΔgltA	-	-	-	-	-	+	-	-	-
ΔgntZ	-	-	-	+	-	-	-	+	+

Fig. 3. Engineering gene knockout mutants for experimental validation of genome-scale metabolic modeling predictions. **A** The flowchart of gene knockout strain development; **b** Isoprenol production and cell growth of constructed gene knockout strains after 48 h using EZ rich medium. Data was obtained from three biological replicates and error bars represent standard deviation.

laboratory evolution to increase growth or a less severe knockdown approach using CRISPRi (Kozaeva et al., 2021) are good candidate approaches to be attempted in the future. The knockout of *aceA* or *gntZ* on the XW15 strain, however, was still producing low levels of isoprenol: 12 mg/L for XW17 strain (Δ*phaABC* Δ*mvaB* Δ*hbdH* Δ*aceA*) and 13 mg/L for XW18 strain (Δ*phaABC* Δ*mvaB* Δ*hbdH* Δ*gntZ*), respectively (Fig. 3b). In the final round of gene knockouts, the XW17 strain was used to integrate the *gntZ* deletion to create the XW19 strain (Δ*phaABC* Δ*mvaB* Δ*hbdH* Δ*aceA* Δ*gntZ*) that contains all gene knockouts that do not affect growth. Interestingly, the inclusion of *gntZ* knockout significantly restored isoprenol production to 114 mg/L (Fig. 3b). Although this isoprenol level was still lower than the two previous strains (XW12 and XW15), it reflects the synergy among multiple gene knockout targets. To understand the different effects caused by Δ*aceA* and/or Δ*gntZ*, we compared the production profiles for XW17 to XW19 strains (Supplementary Fig. 1). It was observed that the XW19 strain depleted glucose after 48 h while the XW17 strain showed 6 g/L residual glucose in the medium. Correspondingly, the cell growth showed the opposite trends in these three strains, such that the XW19 strain showed the highest OD, which is 1.7-fold higher than that of the XW17 strain. However, the effect on cell growth was not directly correlated with the isoprenol yield per consumed glucose for XW17 to XW19 strains (Supplementary Fig. 1).

The growth inhibition by Δ*aceA* or Δ*gntZ* was somewhat unexpected since these genes had no significant fitness in minimal medium conditions with glucose as a carbon source (Thompson et al., 2019). We used the flux balance analysis to investigate whether the effect on cell growth is related to the rich medium setting. For each component in the EZ-rich medium as a sole carbon source, we calculated the maximum growth with and without the *aceA* or *gntZ* deletion. Out of 25 components for which growth can be simulated, 20 components had a decreased maximum growth rate with the *aceA* deletion. However, the *gntZ* deletion did not have an impact on the maximum growth rate. The modeling result for the *aceA* deletion is consistent with a previous observation that the TCA cycle operates under an anaplerotic configuration driven by the glyoxylate shunt in *P. putida* during the early exponential growth on rich medium (Molina et al., 2019). In the same study, isocitrate dehydrogenase was predicted to be inactive during the early and mid-exponential growth where the deletion of *aceA* would significantly reduce the carbon flow through central metabolism. Isocitrate dehydrogenase is also known to be primarily responsible for the NADPH generation in *P. putida* grown on glucose (Nikel et al., 2015). Recently, it was shown that *gntZ* plays a significant role in generating excess NADPH under stress conditions (Nikel et al., 2021). Therefore, combining the *aceA* and *gntZ* deletions would require cells to undergo significant rewiring of central metabolism to overcome the limited carbon flux and NADPH availability.

While the model requires knockout of all targets provided, we instead selected a subset of these targets as ranked by the frequency provided by several methods. The deletion of selected targets still showed significant improvement for isoprenol production even though the model does not predict growth-coupled isoprenol production with a subset. While a correlation analysis between isoprenol production and cell growth (OD$_{600}$) only showed a weak positive correlation (P < 0.05, R^2 = 0.47), it was observed that the higher producers usually showed better cell growth (Supplementary Fig. 2). This suggested that the increased isoprenol production is not at the expense of cell growth at the current isoprenol levels. However, not all strains showed improved isoprenol production and it might be necessary to delete additional genes to achieve a higher yield. For example, the rebound of isoprenol production by integrating both *aceA* and *gntZ* in one strain shows the importance of synergetic effects among different gene targets, which is not well captured by our approach. Such limitation could be alleviated in the future by considering the co-occurrence of gene targets and improving the prioritization method to handle complex or non-intuitive cases better. We also note that the model predictions were made using a minimal medium, whereas experiments were performed using EZ rich defined medium due to better isoprenol production (Wang et al., 2022). Thus, optimizing the production performance in a minimal medium could be a prerequisite to further demonstrate the effectiveness of our frequency-based prioritization of gene targets. Nonetheless, these results show that the deletion of prioritized gene targets can lead to significant improvement in isoprenol production and thus provide support for our computational approach.

In summary, following the genome-scale metabolic modeling recommendations, we constructed single and multiple knockout *P. putida* mutant strains. Among the engineered knockout strains, a triple knockout mutant strain (XW15, Δ*phaABC* Δ*mvaB* Δ*hbdH*) showed the highest isoprenol production (241 mg/L) from EZ rich medium supplemented with 2 % glucose. This demonstrated the utility of computational approaches for host strain optimization to achieve high titer, rate, and yield.

3.3. Pathway optimization for improved isoprenol production

In parallel with the GSMM-guided metabolic rewiring efforts above, we continued to optimize isoprenol pathway gene expression to improve production in *P. putida* KT2440. We first expressed the IPP-bypass isoprenol biosynthetic pathway comprising *mvaE, mvaS, mk,* and *pmd$_{HKQ}$* in different plasmid backbones (Fig. 4a; strains IY781-IY784, Supplementary Table 2) under the control of a LacI repressor in the *P. putida* Δ*phaABC* strain (XW01). The highest titer of 80 mg/L isoprenol was achieved from strain IY782, carrying the isoprenol pathway in the plasmid with the RK2 replication origin (Fig. 4b). Therefore, in the subsequent experiments, plasmid RK2 was used as the expression vector. Since we identified that the arabinose-inducible promoter (P$_{BAD}$) is a stronger promoter than P$_{A1lacO-1}$, (Supplementary Fig. 3) we expressed the isoprenol biosynthetic pathway under the P$_{BAD}$ promoter and replaced the LacI repressor with AraC, in an effort to improve isoprenol production. The absence of the LacI repressor resulted in the constitutive expression of MK and PMD$_{HKQ}$ under a strong P$_{trc-1O}$ promoter (Cook et al., 2018). The resulting strain (IY721) produced up to 395 mg/L isoprenol in 48 h (Fig. 4b). When combined with the GSMM approaches by deleting two genes, *mvaB* and *hbdH*, the resulting strain (IY846) improved the isoprenol production by 1.3-fold when compared to strain IY721, yielding approximately 536 mg/L isoprenol in 48 h (Fig. 4b).

Previous studies in *E. coli* demonstrated that phosphatase overexpression can boost isoprenol production. In our previous paper, we showed that NudB, a native phosphatase of *E. coli*, hydrolyzed IPP and DMAPP into their monophosphate forms, IP and DMAP, respectively, which are subsequently hydrolyzed to isoprenol by other phosphatases such as AphA, Agp, and YqaB (Kang et al., 2016). Among these three phosphatases, AphA was found to best improve the isoprenol titer in *E. coli* (Kang et al., 2016). A recent study for isoprenol production in *S. cerevisiae*, however, reported that co-expressing an *E. coli* alkaline phosphatase, PhoA, produced the highest isoprenol titer (Kim et al., 2021). Therefore, we co-expressed NudB, PhoA, and AphA along with the isoprenol biosynthetic pathway and found that co-expressing AphA alone in the Δ*phaABC* Δ*mvaB* Δ*hbdH* background (strain IY939 with plasmid pIY670) produced the highest isoprenol titer of 1,111 mg/L in 48 h (Fig. 4b).

In an attempt to increase the acetyl-CoA pool, we co-expressed AtoB, NphT7, and/or PMK, and knocked out *ldhA* and *ppsA*. Targeted proteomics confirmed the expression of all proteins (Supplementary Fig. 4), but none of the strains generated higher isoprenol titers compared to strain IY939 (Fig. 4b). Strains co-expressing AphA also accumulated higher biomass compared to those not expressing AphA (Fig. 4c).

3.4. Isoprenol production using optimized isoprenol production pathway and predicted metabolic rewiring in glucose minimal medium

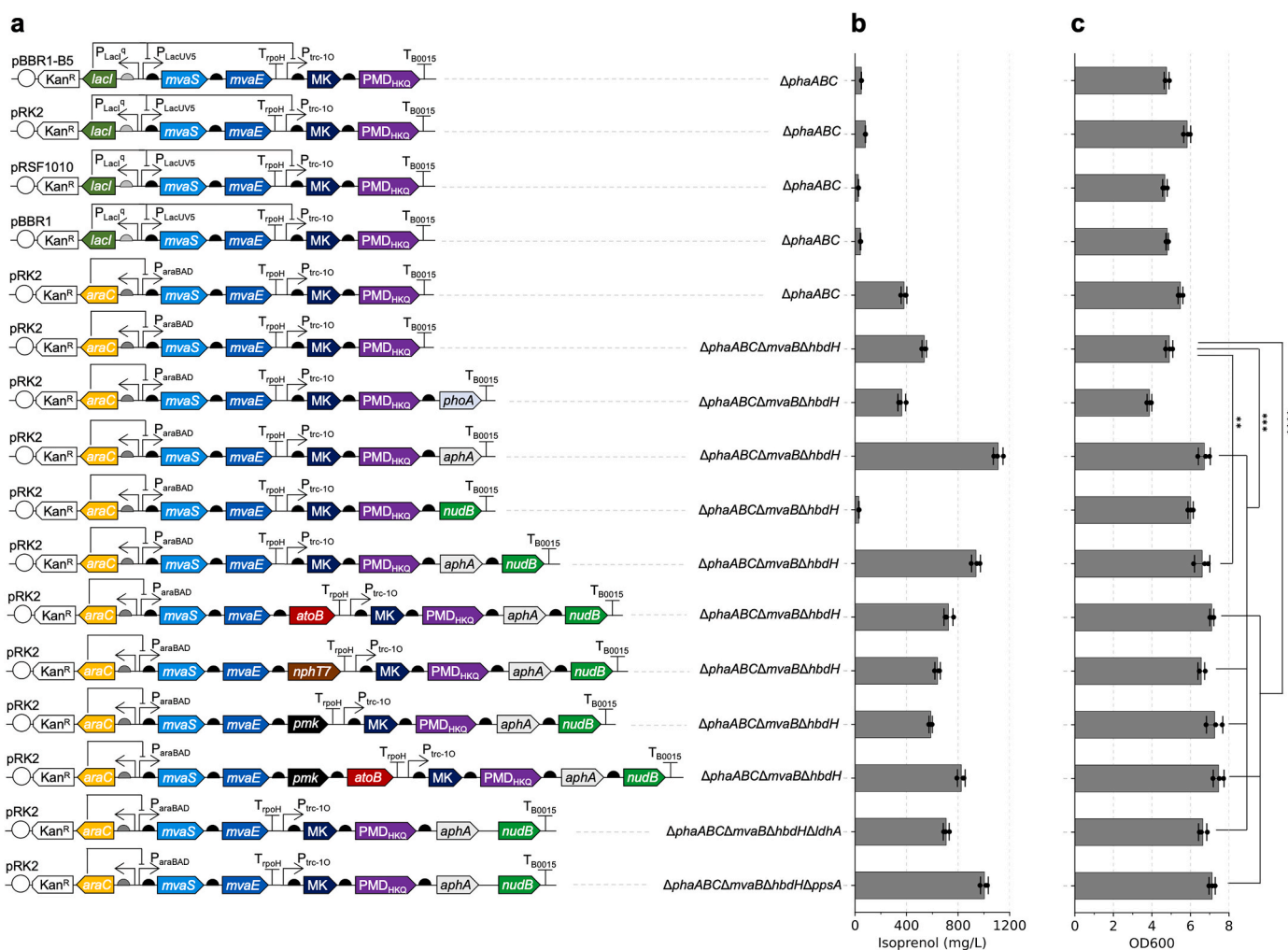Using the optimized isoprenol pathway, we continued to

Fig. 4. Pathway optimization in EZ rich medium. **a** Schematic diagram of plasmids (Supplementary Table 2) used in this study. **b** Isoprenol titer obtained at 48 h from strains transformed with plasmids shown in **a**. **c** Cell density (OD$_{600}$) from strains shown in **b** measured at 48 h. Data were obtained from three biological replicates and error bars represent standard deviation. Asterisks indicate statistical significance by Student's t-test (**, 0.001 < P < 0.01; *** 0.0001 < P < 0.001; ****P < 0.0001).

characterize the engineered strains carrying GSMM-predicted gene knockouts. Defined rich medium such as EZ rich medium contains additional carbon and nitrogen sources (e.g. amino acids) that could trigger complex regulatory mechanisms, such as carbon catabolite repression (Browne et al., 2010; Molina et al., 2019; Moreno et al., 2009). The improved isoprenol production by the optimized pathway now enabled us to characterize the engineered strains in the minimal defined medium used for the GSMM-predicted gene targets. We tested wild-type and fourteen different knockout strains in the pIY670 background for growth and isoprenol production in M9 glucose minimal media plus 20 g/L glucose (Fig. 5). Since we switched from EZ rich medium (several carbon sources) to minimal medium with glucose as the sole carbon source, we deleted an additional gene, PP_2675, to avoid the catabolism of isoprenol after glucose consumption as this gene was reported to be involved in isoprenol degradation (Thompson et al., 2020). We observed that the IY1452 strain (ΔphaABC ΔmvaB ΔhbdH ΔldhA ΔPP_2675 with plasmid pIY670) had the best isoprenol titer at 762 mg/L, Fig. 5); over 4-fold higher than WT (IY1245). The highest isoprenol titer observed was 816 mg/L for the IY1252 strain at 48 h but that reduced by about 70 %–259 mg/L at 72 h. We observed that there was negligible reduction in isoprenol titers in the IY1452 strain at 72 h, unlike the other strains in M9 glucose minimal medium. Interestingly, the deletion of both ldhA and PP_2675 was needed to improve the maximum isoprenol production titer while reducing isoprenol

degradation (Supplementary Fig. 5).

Next, we investigated the growth dynamics, carbon utilization, and isoprenol production profiles of the engineered strains via 72 h time-course profiles of engineered strains in M9 glucose minimal medium. There was no statistical difference in growth rate, and glucose consumption only varied slightly (Fig. 6a). IY1245 (base strain) and IY1261 had similar isoprenol production rates during the glucose consumption phase (up to 42 h) but strains IY1249, IY939, IY1254, and IY1452 had higher rates. IY1452 strain produced isoprenol at 0.34 mmol/gCDW/hr; a 4.69-fold improvement compared to the base strain. Importantly, IY1452 did not degrade isoprenol after glucose was depleted (Fig. 6a).

3.5. Improved isoprenol producing phenotype observed for the IY1452 strain

Context-specific GSMMs were used to investigate the metabolic changes in the engineered strains using the constraints of the gene deletions and phenotypic data (glucose consumption, biomass formation, and isoprenol production rates, Fig. 6b). To compare the metabolic changes between the different engineered strains and WT, through flux redistribution, we performed flux variability analysis (FVA) for each context-specific GSMM. The metabolic flux span was calculated for each of the reactions during optimal growth under the defined constraints and normalized by the glucose uptake rate to compare the variability

	IY1245	IY1261	IY1319	IY1320	IY1246	IY1249	IY1884	IY1250	IY1251	IY1885	IY1252	IY1262	IY1263	IY1254	IY1452
WT	+	-	-	-	-	-	-	-	-	-	-	-	-	-	-
ΔphaABC	-	+	-	-	-	+	+	+	+	+	+	+	+	+	+
ΔmvaB	-	-	+	-	-	+	-	+	+	-	+	+	+	+	+
ΔhbdH	-	-	-	+	-	-	-	-	-	-	+	+	+	+	+
ΔaceA	-	-	-	-	-	-	+	-	-	-	+	-	-	+	-
ΔgntZ	-	-	-	-	-	-	-	+	-	-	-	-	-	+	-
ΔldhA	-	-	-	-	-	-	-	-	-	+	-	+	-	-	+
ΔppsA	-	-	-	-	-	-	-	-	-	-	-	-	+	-	-
PP_2675	-	-	-	-	+	-	+	-	-	+	-	-	-	-	+
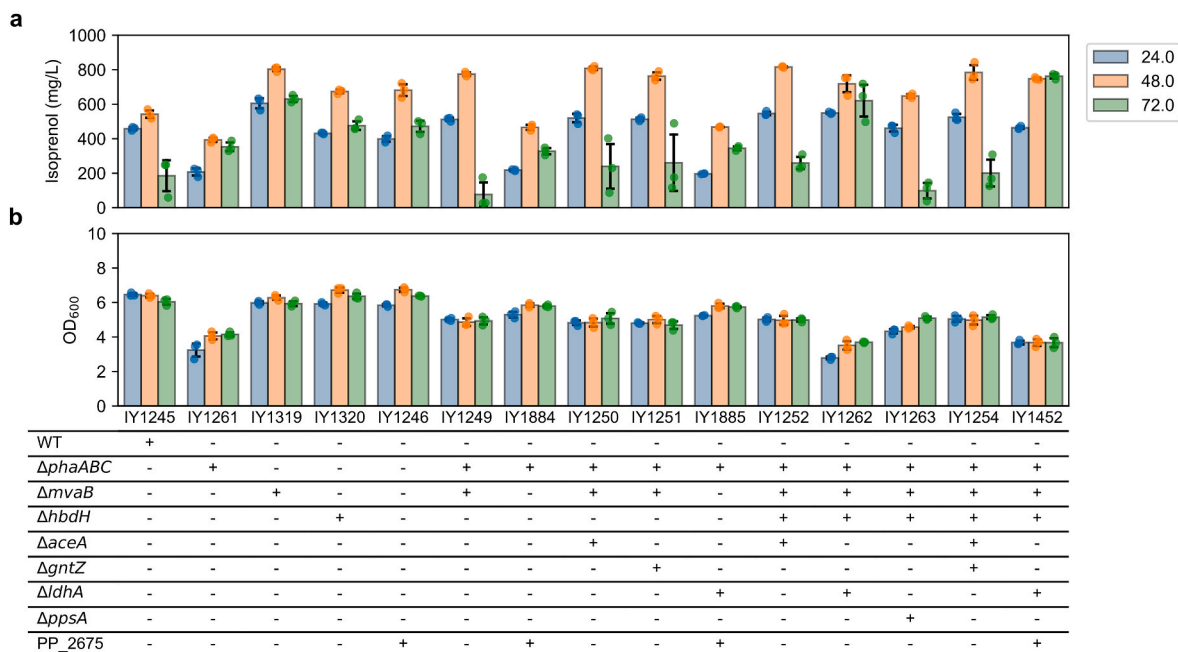
Fig. 5. a Isoprenol production and **b** growth in M9 glucose minimal medium using the optimized isoprenol production plasmid (pIY670, Supplementary Table 1) after double adaptation. Data were obtained from three biological replicates and error bars represent standard deviation.
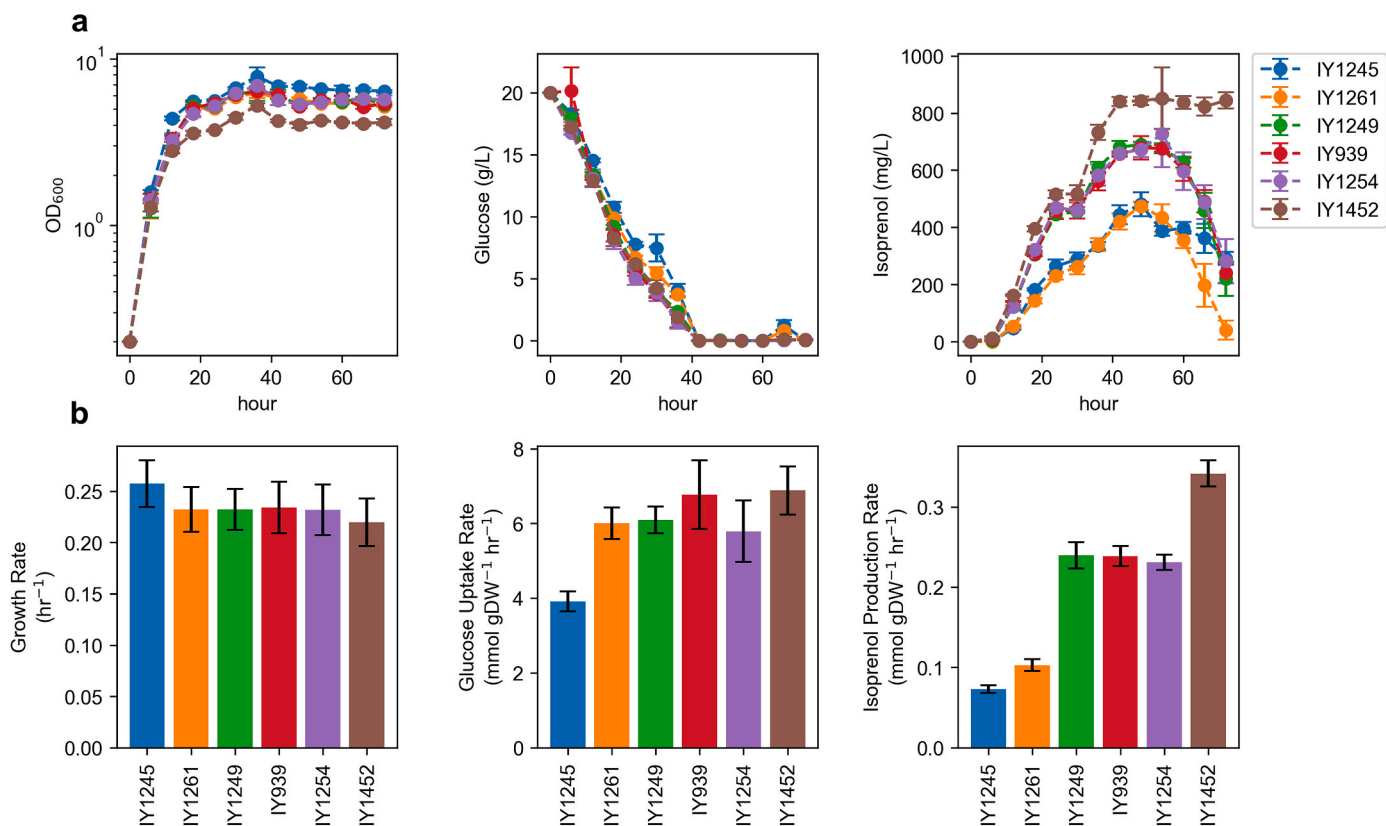
Fig. 6. Time-course profiles of the engineered *P. putida* KT2440 strains in M9 glucose minimal medium. **a** Growth, glucose consumption, and isoprenol production. Data were obtained from three biological replicates and error bars represent standard deviation. **b** Specific rates estimated using the first three time points (0 h, 6 h and 12 h) during exponential growth. Error bars represent the estimated standard error.

across different GSMMs. The flux span corresponds to the flexibility/rigidity of each reaction during maximal growth and isoprenol production based on experimental constraints. A narrow flux span means a rigid flux due to either a causal or correlational effect of the strain engineering for improved isoprenol production indicating very

constrained metabolism at the given isoprenol production level and thus could lead to potential overexpression targets. A narrow flux may also be an effect of the engineering aimed at reducing the carbon flux away from the isoprenol pathway. On the contrary, a wider flux span reflects that these reactions have numerous permissible carbon flux values at the

observed isoprenol production, and some of these reactions are potential deletion targets to further improve isoprenol production.

Selected reactions involving the precursor metabolites with respect to central metabolism and their flux spans are shown in Fig. 7. The FVA of the context-specific GSMM shows that the second reaction in the heterologous IPP-bypass isoprenol production pathway, HMGCOAS (*mvaS*, Reaction 11 in Fig. 7), has a narrow flux span in the strains with additional gene deletions on top of *ΔphaABC*, i.e. strains that have the PP_3540/*mvaB* gene deletion. Given the constraints and assumptions in the GSMM, we can imagine two possible reasons for this narrow flux span in the *ΔmvaB* strains compared to the wider flux span in WT and *ΔphaABC* strains. It could be a result of high flux in competing pathways that redirect carbon flux away from the metabolic pathways of interest to maintain similar growth rates as WT and *ΔphaABC* strains (Fig. 6b, 0.22 hr^{-1} versus 0.26 hr^{-1}) given the limited resources available in M9 glucose minimal medium. Alternatively, the reduction in flux span in strains with *mvaB* deletion is perhaps due to the elimination of a critical degree of freedom, truly constraining the flux profile. Firstly using FVA, we observed a high flux in the HMG-CoA consuming reaction, in case of WT and *ΔphaABC* strains (Reaction 12 in Fig. 7), a competing re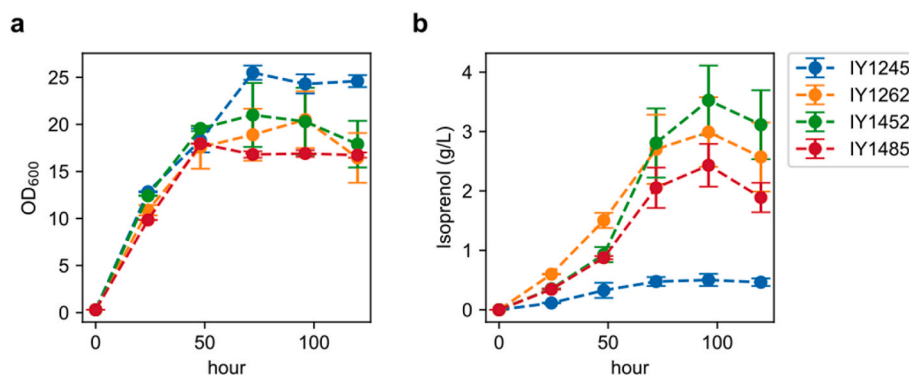action that redirects carbon flux away from the heterologous IPP-bypass pathway. This high allowable flux was reduced by the PP_3540/*mvaB* deletion. Secondly, based on FVA, we observed there was a high flux span in BDH (*hbdH*, Reaction 13 in Fig. 7), in the direction diverting flux towards butanoate metabolism, away from the heterologous IPP-bypass pathway. This was resolved by the PP_3073/*hbdH* deletion on top of the *mvaB* deletion. In the GSMM, ACACT1r (Reaction 10 in Fig. 7) was assumed to have flux only in the direction of IPP-bypass due to additional pIY670 plasmid-borne *mvaE* activity. Zero flux through ACALDtpp (Reaction 2 in Fig. 7) represents reduction in secretion of byproducts such as acetaldehyde.

Although more than 50 % of the reactions carried zero flux under glucose minimal medium conditions, 1304 reactions (45 %) carried a substantial flux (Supplementary Fig. 6). After constraining the model using our experimental data, the best performing strain IY1452 showed substantial fold changes in fluxes although the directionality of the reactions was similar to WT (Supplementary Fig. 7). Of these 1304 reactions, 964 reactions had an increased flux span by more than 1.5-fold compared to WT and were spread across central carbon metabolism and biosynthesis pathways. There were 225 reactions with a reduced flux span ranging from 1 % to 80 % of WT flux magnitudes. 69 of these reactions had 0.5-fold or lower flux and mainly belong to alcohol degradation, butanoate metabolism, and also the HMG-CoA synthase reaction of the IPP-bypass pathway. Additionally, 156 reactions had a flux span reduction between 0.5-fold and 0.8-fold and were shared across non-unique subsystems including alanine and aspartate metabolism, branched amino acid metabolism, fatty acid metabolism, and PHA metabolism.

In summary, when compared to WT, the best performing strain IY1452 showed increased flux through desirable reactions for an increased acetyl-CoA pool (Fig. 7b, reactions 1, 3, 5, 6, and 15) and reduced to negligible flux through competing reactions that redirect carbon flux away from the isoprenol production pathway (Fig. 7b, reactions 2, 8, 12 and 13). A restricted flux span through reactions 11 and 14 points toward future strain engineering to redirect flux from fatty acid metabolism towards HMG-CoA for further improving isoprenol production. A high flux span through citrate synthase (Reaction 4 in Fig. 7) in most of the engineered strains suggests revisiting *gltA* as a target for down-regulation. Although the *gltA* deletion showed a significant growth defect, it was one of the top targets predicted by our computational approach (Table 1) and also previously identified by kinetic modeling as a down-regulation target to increase acetyl-CoA availability in *P. putida* (Kozaeva et al., 2021).

3.6. Isoprenol production in fed-batch cultivation

Four strains (IY1245 (control), IY1262, IY1452, and IY1485) were cultured in fed-batch mode to increase isoprenol titer by supplying additional carbon and nitrogen. After the batch phase with the modified M9 minimal medium containing 20 g/L of glucose and 1.06 g/L (or 20

Fig. 7. Flux variability analysis for the 6 different *P. putida* genotypes/strains with heterologous isoprenol production pathway (pIY670). **a** The central metabolic map is shown with reactions of interest highlighted and the heterologous isoprenol production pathway in green. **b** Flux span normalized to glucose uptake rate for selected reactions.

Fig. 8. Growth and isoprenol production in fed-batch mode. **a** optical density (OD_{600}) and **b** production of isoprenol by IY1245 (wild type), IY1262 ($\Delta phaABC$ $\Delta mvaB$ $\Delta hbdH$ $\Delta ldhA$), IY1452 ($\Delta phaABC$ $\Delta mvaB$ $\Delta hbdH$ $\Delta ldhA$ ΔPP_2675), and IY1485 ($\Delta phaABC$ $\Delta mvaB$ $\Delta hbdH$ $\Delta ldhA$ ΔPP_2675 $\Delta gacA$). The fed-batch productions were performed in the 2 L bioreactors in M9 defined medium in triplicates. Error bars represent standard deviation.

mM) ammonium chloride, the feeding solution was continuously added to make a total of 100 g/L glucose and 2.12 g/L ammonium chloride. As isoprenol evaporates rapidly due to airflow in the bioreactor (Kang et al., 2019), the exhaust line was vented through a bottle containing 1 L oleyl alcohol as a capture solvent to extract isoprenol from the off-gas.

In the IY1245 control strain, the maximum cell growth and the isoprenol production were obtained at 72 h, reaching an OD_{600} of 25.5 ± 0.7 and isoprenol titer of 0.5 ± 0.1 g/L, respectively (Fig. 8). The initial 20 g/L glucose was depleted by 14 h and the isoprenol production was revealed from the off-gas after 24 h, but interestingly, no isoprenol was detected from the culture extract by then (data not shown). This suggests that most isoprenol produced was evaporated by airflow as previously reported in the *E. coli* study (Kang et al., 2019). The IY1262 strain produced 2.3 ± 0.3 g/L of isoprenol and the OD_{600} reached 20.5 ± 3.0 at 96 h (Fig. 8). The growth rate of the engineered strain was slower than the wild-type strain, but the titer was significantly increased. The maximum growth and isoprenol production in the IY1452 strain were obtained, reaching an OD_{600} of 21.0 ± 3.4 at 72 h and a titer of 3.5 ± 0.3 g/L at 96 h (Fig. 8).

Aeration is required in *P. putida* cultivation, but it resulted in a strong foaming, which was difficult to handle even with conventional anti-foaming agents. Furthermore, the excessive foam hinders the use of a standard cultivation protocol (Blesken et al., 2020; Vo et al., 2015). As of now, the precise mechanism for foaming in bioreactors remains poorly understood but at the same time, it is a significant problem during long term bioreactor cultivation. Global regulators such as GacA/GacS, have been reported to have an impact on phenotypes such as attachment,

biofilm formation and other such social behaviors. There have been several known examples in literature. In some cases biofilm can lead to foaming and *lapA* and *lapF* genes are responsible for biofilm formation (López-Sánchez et al., 2016). The two component regulatory system GacA/GacS controls the activity of LapA and other social behaviors (Martínez-Gil et al., 2014). We do not fully understand but a previous report has shown benefits of deleting GacA in *P. putida* under bioreactor conditions (Eng et al., 2021). To reduce foaming during the fed-batch cultivation, the *gacA* gene was deleted in the 5 genes knockout strain (IY1452) as previously reported (Eng et al., 2021). The resulting IY1485 strain reached the OD_{600} of 17.9 ± 0.2 at 48 h and produced 2.4 ± 0.3 g/L of isoprenol at 96 h in fed-batch mode. Even though the *gacA* gene knockout resulted in a significant reduction of foaming, it also resulted in slower growth and lower isoprenol production than the other mutants.

3.7. Isoprenol production using biomass hydrolysate

The use of lignocellulosic biomass for the production of biofuels and bioproducts is of increasing interest (Mohammad and Bhukya, 2022) and *P. putida* is widely recognized for this purpose (Linger et al., 2014; Sodré et al., 2021). Therefore, we evaluated the production of isoprenol by strain IY1452 using a modified M9 minimal medium supplemented with glucose or sorghum hydrolysate as the carbon source. The highest isoprenol titer from this strain was 841 mg/L at 72 h in a modified M9 minimal medium supplemented with 20 g/L of glucose as a sole carbon source (Fig. 9a). Isoprenol production was lower with sorghum
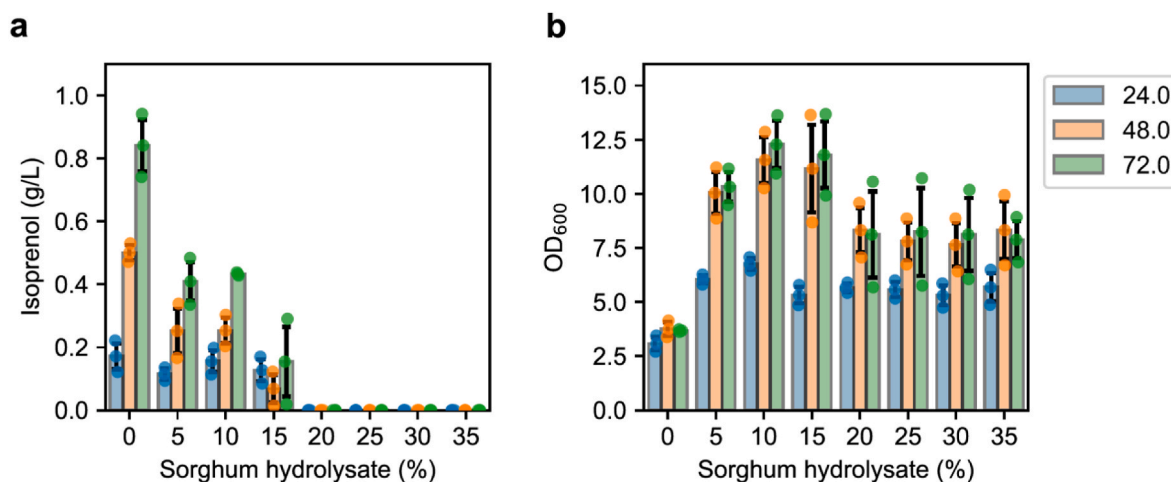

Fig. 9. Isoprenol production and growth using hydrolysate. **a** production of isoprenol by IY1452 and **b** optical density (OD_{600}). The productions of isoprenol and growth were evaluated in the culture tubes in 5 mL modified M9 minimal medium with varying concentrations of hydrolysate in triplicates. Error bars represent standard deviation.

hydrolysate: 409 mg/L and 432 mg/L at 72 h with 5 % and 10 % sorghum hydrolysate, respectively (Fig. 9a). However, it is noteworthy that the growth rates of cultures with sorghum hydrolysate were higher than the growth rate with pure glucose, suggesting additional nutrients in the hydrolysate promoted cell growth (Fig. 9b). Despite the lower isoprenol titers, the culture with sorghum hydrolysate showed promise as an alternative production medium with a higher growth rate than the culture with glucose as the sole carbon source.

Our GSMM-based computational strain design predictions were based on glucose as the sole carbon source under minimal medium cultivation conditions. Sorghum-based hydrolysates are composed of a variety of carbon sources that are further dependent on the pretreatment method (Lim et al., 2020; Park et al., 2020; Sasaki et al., 2019). It is reported that Sorghum-based ionic liquid (cholinium lysinate, [Ch] [Lys]) pretreated hydrolysate consists of glucose, xylose, acetate, and several aromatic compounds (Sasaki et al., 2019). *P. putida* KT2440 lacks the capability to utilize xylose natively but has been reportedly engineered for xylose utilization (Bator et al., 2019; Dvořák and de Lorenzo, 2018; Lim et al., 2021). We observed improvement in growth across all tested fractions of hydrolysate but the isoprenol titers decreased with increasing fraction of hydrolysate in the medium when compared to glucose as the sole carbon source. This can be attributed to the presence of multiple carbon re-routing metabolic pathways towards growth versus limited bioconversion routes towards isoprenol production via the IPP-bypass pathway.

4. Conclusions

Anthropogenic release of carbon into the atmosphere has resulted in climate change, and sustainable aviation fuels (SAFs) offer an effective near-term means of mitigating this continued deleterious carbon release. In this study, we have reported our efforts to engineer strains of *Pseudomonas putida* that can produce the SAF precursor isoprenol from plant-derived carbon sources. We simultaneously pursued rational and GSMM-based target selection approaches followed by engineering and testing in various culture configurations, including fed-batch bioreactors.

Two GSMM approaches were applied, and each predicted a significant number of gene knockout targets in order to realize the computationally predicted improvement in isoprenol yield. Through an ensemble ranking of the myriad gene targets from the two approaches, we were able to prioritize and reduce the total number of targets. This approach proved fruitful in decreasing the number of engineered strains needed to realize a significant improvement in titer and rate. However, we also observed that some of the predictions did not result in titer improvements, and some combinations of knockouts were detrimental to *P. putida* growth and/or isoprenol titers. Rational pathway optimization had a significant impact on titer improvement. The synergistic application of GSMM-guided gene knockouts and rational pathway optimization led to the highest titer of isoprenol in *P. putida* at 1.1 g/L; a 10-fold improvement vs. the starting strain. Fed-batch cultivation further improved the titer to 3.5 g/L.

Since knocking-out multiple genes in *P. putida* is not a trivial amount of effort, and the knock-outs frequently result in growth retardation, gene knock-downs could be an alternative to gene knock-out to screen multiple combinations of target genes. Application of CRISPR interference and building an automated process may accelerate rapid strain engineering to improve isoprenol TRY. Further, adaptive laboratory evolution (ALE)-based tolerization (Lim et al., 2020) and other state-of-the-art strain engineering techniques (Elmore et al., 2020; Lim et al., 2021) can be applied to further improve isoprenol titers, rates, and yields in future research. For ultimate industrial applications, additional improvements must be made, including further genetic engineering strain improvements, bioprocess optimization, and separations process engineering to include downstream recovery of the volatile product.

Code availability

All custom computer code used to generate the results reported in this manuscript are available via the Jupyter Notebooks and Supplementary Information provided along with this manuscript.

CRediT authorship contribution statement

Deepanwita Banerjee: Conceptualization, Data curation, Formal analysis, Investigation, Methodology, Visualization, Writing – original draft, Writing – review & editing. **Ian S. Yunus:** Conceptualization, Data curation, Formal analysis, Investigation, Methodology, Visualization, Writing – original draft, Writing – review & editing. **Xi Wang:** Conceptualization, Data curation, Formal analysis, Investigation, Methodology, Visualization, Writing – original draft, Writing – review & editing. **Jinho Kim:** Investigation, Methodology, Writing – original draft, Writing – review & editing. **Aparajitha Srinivasan:** Investigation, Methodology. **Russel Menchavez:** Investigation, Methodology. **Yan Chen:** Investigation, Methodology. **Jennifer W. Gin:** Investigation, Methodology. **Christopher J. Petzold:** Investigation, Methodology, Writing – original draft. **Hector Garcia Martin:** Writing – review & editing. **Jon K. Magnuson:** Writing – review & editing. **Paul D. Adams:** Writing – review & editing. **Blake A. Simmons:** Funding acquisition, Writing – review & editing. **Aindrila Mukhopadhyay:** Conceptualization, Funding acquisition, Supervision, Writing – original draft, Writing – review & editing. **Joonhoon Kim:** Conceptualization, Data curation, Formal analysis, Investigation, Methodology, Supervision, Visualization, Writing – original draft, Writing – review & editing. **Taek Soon Lee:** Conceptualization, Data curation, Funding acquisition, Project administration, Supervision, Writing – original draft, Writing – review & editing.

Declaration of competing interest

The authors declare no competing interests.

Data availability

Data will be made available on request.

Acknowledgements

Appendix A. Supplementary data

Supplementary data to this article can be found online at https://doi.org/10.1016/j.ymben.2024.02.004.

References

Baral, N.R., Kavvada, O., Mendez-Perez, D., Mukhopadhyay, A., Lee, T.S., Simmons, B.A., Scown, C.D., 2019a. Techno-economic analysis and life-cycle greenhouse gas mitigation cost of five routes to bio-jet fuel blendstocks. Energy Environ. Sci. 12, 807–824. https://doi.org/10.1039/C8EE03266A.

Baral, N.R., Sundstrom, E.R., Das, L., Gladden, J.M., Eudes, A., Mortimer, J., Singer, S.W., Mukhopadhyay, A., Scown, C.D., 2019b. Approaches for more efficient biological conversion of lignocellulosic feedstocks to biofuels and bioproducts. ACS Sustain. Chem. Eng. 7, 9062–9079. https://doi.org/10.1021/acssuschemeng.9b01229.

Baral, N.R., Yang, M., Harvey, B.G., Simmons, B.A., Mukhopadhyay, A., Lee, T.S., Scown, C.D., 2021. Production cost and carbon footprint of biomass-derived dimethylcyclooctane as a high-performance jet fuel blendstock. ACS Sustain. Chem. Eng. 9, 11872–11882. https://doi.org/10.1021/acssuschemeng.1c03772.

Bator, I., Wittgens, A., Rosenau, F., Tiso, T., Blank, L.M., 2019. Comparison of three xylose pathways in Pseudomonas putidaKT2440 for the synthesis of valuable products. Front. Bioeng. Biotechnol. 7, 480. https://doi.org/10.3389/fbioe.2019.00480.

Blesken, C.C., Bator, I., Eberlein, C., Heipieper, H.J., Tiso, T., Blank, L.M., 2020. Genetic cell-surface modification for optimized foam fractionation. Front. Bioeng. Biotechnol. 8, 572892 https://doi.org/10.3389/fbioe.2020.572892.

Browne, P., Barret, M., O'Gara, F., Morrissey, J.P., 2010. Computational prediction of the Crc regulon identifies genus-wide and species-specific targets of catabolite repression control in Pseudomonas bacteria. BMC Microbiol. 10, 300. https://doi.org/10.1186/1471-2180-10-300.

Bujdoš, D., Popelářová, B., Volke, D.C., Nikel, P.I., Sonnenschein, N., Dvořák, P., 2023. Engineering of Pseudomonas putida for accelerated co-utilization of glucose and cellobiose yields aerobic overproduction of pyruvate explained by an upgraded metabolic model. Metab. Eng. 75, 29–46. https://doi.org/10.1016/j.ymben.2022.10.011.

Burgard, A.P., Pharkya, P., Maranas, C.D., 2003. Optknock: a bilevel programming framework for identifying gene knockout strategies for microbial strain optimization. Biotechnol. Bioeng. 84, 647–657. https://doi.org/10.1002/bit.10803.

Chen, Y., Guenther, J.M., Gin, J.W., Chan, L.J.G., Costello, Z., Ogorzalek, T.L., Tran, H. M., Blake-Hedges, J.M., Keasling, J.D., Adams, P.D., García Martín, H., Hillson, N.J., Petzold, C.J., 2019a. Automated "cells-to-peptides" sample preparation workflow for high-throughput, quantitative proteomic assays of microbes. J. Proteome Res. 18, 3752–3761. https://doi.org/10.1021/acs.jproteome.9b00455.

Chen, Y., Vu, J., Thompson, M.G., Sharpless, W.A., Chan, L.J.G., Gin, J.W., Keasling, J.D., Adams, P.D., Petzold, C.J., 2019b. A rapid methods development workflow for high-throughput quantitative proteomic applications. PLoS One 14, e0211582. https://doi.org/10.1371/journal.pone.0211582.

Cook, T.B., Rand, J.M., Nurani, W., Courtney, D.K., Liu, S.A., Pfleger, B.F., 2018. Genetic tools for reliable gene expression and recombineering in Pseudomonas putida. J. Ind. Microbiol. Biotechnol. 45, 517–527. https://doi.org/10.1007/s10295-017-2001-5.

Cruz-Morales, P., Yin, K., Landera, A., Cort, J.R., Young, R.P., Kyle, J.E., Bertrand, R., Iavarone, A.T., Acharya, S., Cowan, A., Chen, Y., Gin, J.W., Scown, C.D., Petzold, C. J., Araujo-Barcelos, C., Sundstrom, E., George, A., Liu, Y., Klass, S., Nava, A.A., Keasling, J.D., 2022. Biosynthesis of polycyclopropanated high energy biofuels. Joule 6, 1590–1605. https://doi.org/10.1016/j.joule.2022.05.011.

Czajka, J.J., Banerjee, D., Eng, T., Menasalvas, J., Yan, C., Munoz, N.M., Poirier, B.C., Kim, Y.-M., Baker, S.E., Tang, Y.J., Mukhopadhyay, A., 2022. Tuning a high performing multiplexed-CRISPRi Pseudomonas putida strain to further enhance indigoidine production. Metab. Eng. Commun. 15, e00206 https://doi.org/10.1016/j.mec.2022.e00206.

Department of Energy, U.S., 2021. Co-Optimization of Fuels & Engines Year in Review (FY20). EERE Publication and Product Library. https://doi.org/10.2172/1782424.

Dong, J., Chen, Y., Benites, V.T., Baidoo, E.E.K., Petzold, C.J., Beller, H.R., Eudes, A., Scheller, H.V., Adams, P.D., Mukhopadhyay, A., Simmons, B.A., Singer, S.W., 2019. Methyl ketone production by Pseudomonas putida is enhanced by plant-derived amino acids. Biotechnol. Bioeng. 116, 1909–1922. https://doi.org/10.1002/bit.26995.

Dvořák, P., de Lorenzo, V., 2018. Refactoring the upper sugar metabolism of Pseudomonas putida for co-utilization of cellobiose, xylose, and glucose. Metab. Eng. 48, 94–108. https://doi.org/10.1016/j.ymben.2018.05.019.

Ebrahim, A., Lerman, J.A., Palsson, B.O., Hyduke, D.R., 2013. COBRApy: COnstraints-based reconstruction and analysis for Python. BMC Syst. Biol. 7, 74. https://doi.org/10.1186/1752-0509-7-74.

Elmore, J.R., Dexter, G.N., Salvachúa, D., O'Brien, M., Klingeman, D.M., Gorday, K., Michener, J.K., Peterson, D.J., Beckham, G.T., Guss, A.M., 2020. Engineered Pseudomonas putida simultaneously catabolizes five major components of corn stover lignocellulose: glucose, xylose, arabinose, p-coumaric acid, and acetic acid. Metab. Eng. 62, 62–71. https://doi.org/10.1016/j.ymben.2020.08.001.

Eng, T., Banerjee, D., Lau, A.K., Bowden, E., Herbert, R.A., Trinh, J., Prahl, J.-P., Deutschbauer, A., Tanjore, D., Mukhopadhyay, A., 2021. Engineering Pseudomonas putida for efficient aromatic conversion to bioproduct using high throughput screening in a bioreactor. Metab. Eng. 66, 229–238. https://doi.org/10.1016/j.ymben.2021.04.015.

Erickson, E., Bleem, A., Kuatsjah, E., Werner, A.Z., DuBois, J.L., McGeehan, J.E., Eltis, L. D., Beckham, G.T., 2022. Critical enzyme reactions in aromatic catabolism for microbial lignin conversion. Nat. Catal. 5, 86–98. https://doi.org/10.1038/s41929-022-00747-w.

Gao, X., Gao, F., Liu, D., Zhang, H., Nie, X., Yang, C., 2016. Engineering the methylerythritol phosphate pathway in cyanobacteria for photosynthetic isoprene production from CO2. Energy Environ. Sci. 9, 1400–1411. https://doi.org/10.1039/C5EE03102H.

Geiselman, G.M., Kirby, J., Landera, A., Otoupal, P., Papa, G., Barcelos, C., Sundstrom, E. R., Das, G., Magurudeniya, H.D., Wehrs, M., Rodriguez, A., Simmons, B.A., Magnuson, J.K., Mukhopadhyay, A., Lee, T.S., George, A., Gladden, J.M., 2020. Conversion of poplar biomass into high-energy density tricyclic sesquiterpene jet fuel blendstocks. Microb. Cell Factories 19, 208. https://doi.org/10.1186/s12934-020-01456-4.

Heirendt, L., Arreckx, S., Pfau, T., Mendoza, S.N., Richelle, A., Heinken, A., Haraldsdóttir, H.S., Wachowiak, J., Keating, S.M., Vlasov, V., Magnusdóttir, S., Ng, C.Y., Preciat, G., Žagare, A., Chan, S.H.J., Aurich, M.K., Clancy, C.M., Modamio, J., Sauls, J.T., Noronha, A., Fleming, R.M.T., 2019. Creation and analysis of biochemical constraint-based models using the COBRA Toolbox v.3.0. Nat. Protoc. 14, 639–702. https://doi.org/10.1038/s41596-018-0098-2.

Hernandez-Arranz, S., Perez-Gil, J., Marshall-Sabey, D., Rodriguez-Concepcion, M., 2019. Engineering Pseudomonas putida for isoprenoid production by manipulating endogenous and shunt pathways supplying precursors. Microb. Cell Factories 18, 152. https://doi.org/10.1186/s12934-019-1204-z.

Kang, A., George, K.W., Wang, G., Baidoo, E., Keasling, J.D., Lee, T.S., 2016. Isopentenyl diphosphate (IPP)-bypass mevalonate pathways for isopentenol production. Metab. Eng. 34, 25–35. https://doi.org/10.1016/j.ymben.2015.12.002.

Kang, A., Mendez-Perez, D., Goh, E.-B., Baidoo, E.E.K., Benites, V.T., Beller, H.R., Keasling, J.D., Adams, P.D., Mukhopadhyay, A., Lee, T.S., 2019. Optimization of the IPP-bypass mevalonate pathway and fed-batch fermentation for the production of isoprenol in Escherichia coli. Metab. Eng. 56, 85–96. https://doi.org/10.1016/j.ymben.2019.09.003.

Keasling, J., Garcia Martin, H., Lee, T.S., Mukhopadhyay, A., Singer, S.W., Sundstrom, E., 2021. Microbial production of advanced biofuels. Nat. Rev. Microbiol. 19, 701–715. https://doi.org/10.1038/s41579-021-00577-w.

Kim, J., Baidoo, E.E.K., Amer, B., Mukhopadhyay, A., Adams, P.D., Simmons, B.A., Lee, T.S., 2021. Engineering Saccharomyces cerevisiae for isoprenol production. Metab. Eng. 64, 154–166. https://doi.org/10.1016/j.ymben.2021.02.002.

Klamt, S., Saez-Rodriguez, J., Gilles, E.D., 2007. Structural and functional analysis of cellular networks with CellNetAnalyzer. BMC Syst. Biol. 1, 2. https://doi.org/10.1186/1752-0509-1-2.

Korz, D.J., Rinas, U., Hellmuth, K., Sanders, E.A., Deckwer, W.D., 1995. Simple fed-batch technique for high cell density cultivation of Escherichia coli. J. Biotechnol. 39, 59–65. https://doi.org/10.1016/0168-1656(94)00143-Z.

Kozaeva, E., Volkova, S., Matos, M.R.A., Mezzina, M.P., Wulff, T., Volke, D.C., Nielsen, L. K., Nikel, P.I., 2021. Model-guided dynamic control of essential metabolic nodes boosts acetyl-coenzyme A-dependent bioproduction in rewired Pseudomonas putida. Metab. Eng. 67, 373–386. https://doi.org/10.1016/j.ymben.2021.07.014.

Kukurugya, M.A., Mendonca, C.M., Solhtalab, M., Wilkes, R.A., Thannhauser, T.W., Aristilde, L., 2019. Multi-omics analysis unravels a segregated metabolic flux network that tunes co-utilization of sugar and aromatic carbons in Pseudomonas putida. J. Biol. Chem. 294, 8464–8479. https://doi.org/10.1074/jbc.RA119.007885.

Liew, F.E., Nogle, R., Abdalla, T., Rasor, B.J., Canter, C., Jensen, R.O., Wang, L., Strutz, J., Chirania, P., De Tissera, S., Mueller, A.P., Ruan, Z., Gao, A., Tran, L., Engle, N.L., Bromley, J.C., Daniell, J., Conrado, R., Tschaplinski, T.J., Giannone, R. J., Köpke, M., 2022. Carbon-negative production of acetone and isopropanol by gas fermentation at industrial pilot scale. Nat. Biotechnol. 40, 335–344. https://doi.org/10.1038/s41587-021-01195-w.

Lim, H.G., Eng, T., Banerjee, D., Alarcon, G., Lau, A.K., Park, M.-R., Simmons, B.A., Palsson, B.O., Singer, S.W., Mukhopadhyay, A., Feist, A.M., 2021. Generation of Pseudomonas putidaKT2440 strains with efficient utilization of xylose and galactose via adaptive laboratory evolution. ACS Sustain. Chem. Eng. 9, 11512–11523. https://doi.org/10.1021/acssuschemeng.1c03765.

Lim, H.G., Fong, B., Alarcon, G., Magurudeniya, H.D., Eng, T., Szubin, R., Olson, C.A., Palsson, B.O., Gladden, J.M., Simmons, B.A., Mukhopadhyay, A., Singer, S.W., Feist, A.M., 2020. Generation of ionic liquid tolerant Pseudomonas putida KT2440 strains via adaptive laboratory evolutions. Green Chem. 22, 5677–5690. https://doi.org/10.1039/D0GC01663B.

Linger, J.G., Vardon, D.R., Guarnieri, M.T., Karp, E.M., Hunsinger, G.B., Franden, M.A., Johnson, C.W., Chupka, G., Strathmann, T.J., Pienkos, P.T., Beckham, G.T., 2014. Lignin valorization through integrated biological funneling and chemical catalysis. Proc. Natl. Acad. Sci. U.S.A. 111, 12013–12018. https://doi.org/10.1073/pnas.1410657111.

Liu, C.-L., Tian, T., Alonso-Gutierrez, J., Garabedian, B., Wang, S., Baidoo, E.E.K., Benites, V., Chen, Y., Petzold, C.J., Adams, P.D., Keasling, J.D., Tan, T., Lee, T.S., 2018. Renewable production of high density jet fuel precursor sesquiterpenes from Escherichia coli. Biotechnol. Biofuels 11, 285. https://doi.org/10.1186/s13068-018-1272-z.

López-Sánchez, A., Leal-Morales, A., Jiménez-Díaz, L., Platero, A.I., Bardallo-Pérez, J., Díaz-Romero, A., Acemel, R.D., Illán, J.M., Jiménez-López, J., Govantes, F., 2016. Biofilm formation-defective mutants in Pseudomonas putida. FEMS Microbiol. Lett. 363 https://doi.org/10.1093/femsle/fnw127.

Magurudeniya, H.D., Baral, N.R., Rodriguez, A., Scown, C.D., Dahlberg, J., Putnam, D., George, A., Simmons, B.A., Gladden, J.M., 2021. Use of ensiled biomass sorghum increases ionic liquid pretreatment efficiency and reduces biofuel production cost and carbon footprint. Green Chem. 23, 3127–3140. https://doi.org/10.1039/D0GC03260C.

Maia, P., Rocha, M., Rocha, I., 2016. In silico constraint-based strain optimization methods: the quest for optimal cell factories. Microbiol. Mol. Biol. Rev. 80, 45–67. https://doi.org/10.1128/MMBR.00014-15.

Martínez-García, E., de Lorenzo, V., 2019. Pseudomonas putida in the quest of programmable chemistry. Curr. Opin. Biotechnol. 59, 111–121. https://doi.org/10.1016/j.copbio.2019.03.012.

Martínez-Gil, M., Ramos-González, M.I., Espinosa-Urgel, M., 2014. Roles of cyclic Di-GMP and the Gac system in transcriptional control of the genes coding for the Pseudomonas putida adhesins LapA and LapF. J. Bacteriol. 196, 1484–1495. https://doi.org/10.1128/JB.01287-13.

Marx, C.J., 2008. Development of a broad-host-range sacB-based vector for unmarked allelic exchange. BMC Res. Notes 1, 1. https://doi.org/10.1186/1756-0500-1-1.

Mohammad, S.H., Bhukya, B., 2022. Biotransformation of toxic lignin and aromatic compounds of lignocellulosic feedstock into eco-friendly biopolymers by Pseudomonas putida KT2440. Bioresour. Technol. 363, 128001 https://doi.org/10.1016/j.biortech.2022.128001.

Molina, L., La Rosa, R., Nogales, J., Rojo, F., 2019. Influence of the Crc global regulator on substrate uptake rates and the distribution of metabolic fluxes in Pseudomonas putida KT2440 growing in a complete medium. Environ. Microbiol. 21, 4446–4459. https://doi.org/10.1111/1462-2920.14812.

Moreno, R., Martínez-Gomariz, M., Yuste, L., Gil, C., Rojo, F., 2009. The Pseudomonas putida Crc global regulator controls the hierarchical assimilation of amino acids in a complete medium: evidence from proteomic and genomic analyses. Proteomics 9, 2910–2928. https://doi.org/10.1002/pmic.200800918.

Nikel, P.I., Chavarría, M., Fuhrer, T., Sauer, U., de Lorenzo, V., 2015. Pseudomonas putida strain metabolizes glucose through a cycle formed by enzymes of the entner-doudoroff, embden-meyerhof-parnas, and pentose phosphate pathways. J. Biol. Chem. 290, 25920–25932. https://doi.org/10.1074/jbc.M115.687749.

Nikel, P.I., de Lorenzo, V., 2018. Pseudomonas putida as a functional chassis for industrial biocatalysis: from native biochemistry to trans-metabolism. Metab. Eng. 50, 142–155. https://doi.org/10.1016/j.ymben.2018.05.005.

Nikel, P.I., Fuhrer, T., Chavarría, M., Sánchez-Pascuala, A., Sauer, U., de Lorenzo, V., 2021. Reconfiguration of metabolic fluxes in Pseudomonas putida as a response to sub-lethal oxidative stress. ISME J. 15, 1751–1766. https://doi.org/10.1038/s41396-020-00884-9.

Nogales, J., Mueller, J., Gudmundsson, S., Canalejo, F.J., Duque, E., Monk, J., Feist, A. M., Ramos, J.L., Niu, W., Palsson, B.O., 2020. High-quality genome-scale metabolic modelling of Pseudomonas putidahighlights its broad metabolic capabilities. Environ. Microbiol. 22, 255–269. https://doi.org/10.1111/1462-2920.14843.

Ouyang, S.-P., Liu, Q., Fang, L., Chen, G.-Q., 2007. Construction of pha-operon-defined knockout mutants of Pseudomonas putida KT2442 and their applications in poly (hydroxyalkanoate) production. Macromol. Biosci. 7, 227–233. https://doi.org/10.1002/mabi.200600187.

Park, M., Chen, Y., Thompson, M., Benites, V.T., Fong, B., Petzold, C.J., Baidoo, E.E.K., Gladden, J.M., Adams, P.D., Keasling, J.D., Simmons, B.A., Singer, S.W., 2020. Response of Pseudomonas putida to complex, aromatic-rich fractions from biomass. ChemSusChem 13, 1–14. https://doi.org/10.1002/cssc.202000268.

Rand, J.M., Pisithkul, T., Clark, R.L., Thiede, J.M., Mehrer, C.R., Agnew, D.E., Campbell, C.E., Markley, A.L., Price, M.N., Ray, J., Wetmore, K.M., Suh, Y., Arkin, A. P., Deutschbauer, A.M., Amador-Noguez, D., Pfleger, B.F., 2017. A metabolic pathway for catabolizing levulinic acid in bacteria. Nat. Microbiol. 2, 1624–1634. https://doi.org/10.1038/s41564-017-0028-z.

Ranganathan, S., Suthers, P.F., Maranas, C.D., 2010. OptForce: an optimization procedure for identifying all genetic manipulations leading to targeted overproductions. PLoS Comput. Biol. 6, e1000744 https://doi.org/10.1371/journal.pcbi.1000744.

Salvachúa, D., Rydzak, T., Auwae, R., De Capite, A., Black, B.A., Bouvier, J.T., Cleveland, N.S., Elmore, J.R., Huenemann, J.D., Katahira, R., Michener, W.E., Peterson, D.J., Rohrer, H., Vardon, D.R., Beckham, G.T., Guss, A.M., 2020. Metabolic engineering of Pseudomonas putida for increased polyhydroxyalkanoate production from lignin. Microb. Biotechnol. 13, 290–298. https://doi.org/10.1111/1751-7915.13481.

Sasaki, Y., Eng, T., Herbert, R.A., Trinh, J., Chen, Y., Rodriguez, A., Gladden, J., Simmons, B.A., Petzold, C.J., Mukhopadhyay, A., 2019. Engineering Corynebacterium glutamicum to produce the biogasoline isopentenol from plant biomass hydrolysates. Biotechnol. Biofuels 12, 41. https://doi.org/10.1186/s13068-019-1381-3.

Segrè, D., Vitkup, D., Church, G.M., 2002. Analysis of optimality in natural and perturbed metabolic networks. Proc. Natl. Acad. Sci. U.S.A. 99, 15112–15117. https://doi.org/10.1073/pnas.232349399.

Sharma, V., Eckels, J., Taylor, G.K., Shulman, N.J., Stergachis, A.B., Joyner, S.A., Yan, P., Whiteaker, J.R., Halusa, G.N., Schilling, B., Gibson, B.W., Colangelo, C.M., Paulovich, A.G., Carr, S.A., Jaffe, J.D., MacCoss, M.J., MacLean, B., 2014. Panorama: a targeted proteomics knowledge base. J. Proteome Res. 13, 4205–4210. https://doi.org/10.1021/pr5006636.

Sodré, V., Vilela, N., Tramontina, R., Squina, F.M., 2021. Microorganisms as bioabatement agents in biomass to bioproducts applications. Biomass Bioenergy 151, 106161. https://doi.org/10.1016/j.biombioe.2021.106161.

Sudarsan, S., Blank, L.M., Dietrich, A., Vielhauer, O., Takors, R., Schmid, A., Reuss, M., 2016. Dynamics of benzoate metabolism in Pseudomonas putida KT2440. Metab. Eng. Commun. 3, 97–110. https://doi.org/10.1016/j.meteno.2016.03.005.

Terzer, M., Stelling, J., 2008. Large-scale computation of elementary flux modes with bit pattern trees. Bioinformatics 24, 2229–2235. https://doi.org/10.1093/bioinformatics/btn401.

Thompson, M.G., Blake-Hedges, J.M., Cruz-Morales, P., Barajas, J.F., Curran, S.C., Eiben, C.B., Harris, N.C., Benites, V.T., Gin, J.W., Sharpless, W.A., Twigg, F.F., Skyrud, W., Krishna, R.N., Pereira, J.H., Baidoo, E.E.K., Petzold, C.J., Adams, P.D., Arkin, A.P., Deutschbauer, A.M., Keasling, J.D., 2019. Massively parallel fitness profiling reveals multiple novel enzymes in Pseudomonas putida lysine metabolism. mBio 10. https://doi.org/10.1128/mBio.02577-18.

Thompson, M.G., Incha, M.R., Pearson, A.N., Schmidt, M., Sharpless, W.A., Eiben, C.B., Cruz-Morales, P., Blake-Hedges, J.M., Liu, Y., Adams, C.A., Haushalter, R.W., Krishna, R.N., Lichtner, P., Blank, L.M., Mukhopadhyay, A., Deutschbauer, A.M., Shih, P.M., Keasling, J.D., 2020. Fatty acid and alcohol metabolism in Pseudomonas putida: functional analysis using random barcode transposon sequencing. Appl. Environ. Microbiol. 86, e01665-20 https://doi.org/10.1128/AEM.01665-20.

Tian, T., Kang, J.W., Kang, A., Lee, T.S., 2019. Redirecting metabolic flux via combinatorial multiplex CRISPRi-mediated repression for isopentenol production in Escherichia coli. ACS Synth. Biol. 8, 391–402. https://doi.org/10.1021/acssynbio.8b00429.

von Kamp, A., Klamt, S., 2017. Growth-coupled overproduction is feasible for almost all metabolites in five major production organisms. Nat. Commun. 8, 15956 https://doi.org/10.1038/ncomms15956.

Vo, M.T., Ko, K., Ramsay, B., 2015. Carbon-limited fed-batch production of medium-chain-length polyhydroxyalkanoates by a phaZ-knockout strain of Pseudomonas putida KT2440. J. Ind. Microbiol. Biotechnol. 42, 637–646. https://doi.org/10.1007/s10295-014-1574-5.

Wang, X., Baidoo, E.E.K., Kakumanu, R., Xie, S., Mukhopadhyay, A., Lee, T.S., 2022. Engineering isoprenoids production in metabolically versatile microbial host Pseudomonas putida. Biotechnol. Biofuels Bioprod. 15, 137. https://doi.org/10.1186/s13068-022-02235-6.

Weiland, F., Kohlstedt, M., Wittmann, C., 2022. Guiding stars to the field of dreams: metabolically engineered pathways and microbial platforms for a sustainable lignin-based industry. Metab. Eng. 71, 13–41. https://doi.org/10.1016/j.ymben.2021.11.011.

Weimer, A., Kohlstedt, M., Volke, D.C., Nikel, P.I., Wittmann, C., 2020. Industrial biotechnology of Pseudomonas putida: advances and prospects. Appl. Microbiol. Biotechnol. 104, 7745–7766. https://doi.org/10.1007/s00253-020-10811-9.